Detonation Diffraction Through a Mixture Gradient

E. Schultz, J. Shepherd

Graduate Aeronautical Laboratories
California Institute of Technology
Pasadena, CA 91125

Explosion Dynamics Laboratory Report FM00-1

February 8, 2000

Contents

Acknowledgements

Funding for this effort has been provided by the National Defense Science and Engineering Graduate Fellowship Program and the NASA Phase I Small Business Technology Transfer Program “Initiators for Pulse Detonation Engines” (NASA-97291) collaboration with Advanced Projects Research, Inc (APRI).

1 Introduction

A simple one-dimensional model of a self-propagating gaseous detonation consists of a shock wave tightly coupled to a reaction zone, propagating through a combustible gas mixture as shown in Fig. 1 (Strehlow 1984). A feedback mechanism exists in that the shock wave generates the thermodynamic conditions under which the gas combusts, and the energy release from the reaction zone maintains the strength of the shock This is in contrast to a flame, or deflagrative combustion, in which thermal and species transport processes dominate. Given a particular set of initial conditions, a self-propagating detonation wave travels at a constant Chapman-Jouguet velocity (V_{CJ}) on the order of a few thousand meters per second, with associated pressures and temperatures of tens of bar and several thousand degrees, respectively. A detonation is actually a three-dimensional shock-reaction zone complex with a dynamic wavefront composed of curved incident, mach stem, and transverse shock waves as depicted in Fig. 2 (Strehlow 1970). The transverse shocks sweep across the wavefront and the triple-point paths form a diamond-shaped cellular pattern. The cell width λ is a characteristic length scale of detonations, indicative of the coupling between gasdynamic and chemical processes.

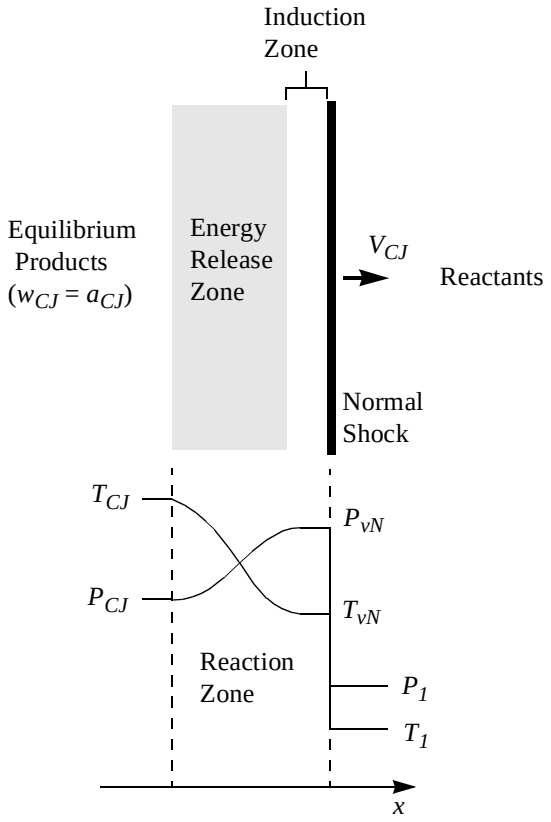

(a) ZND model.

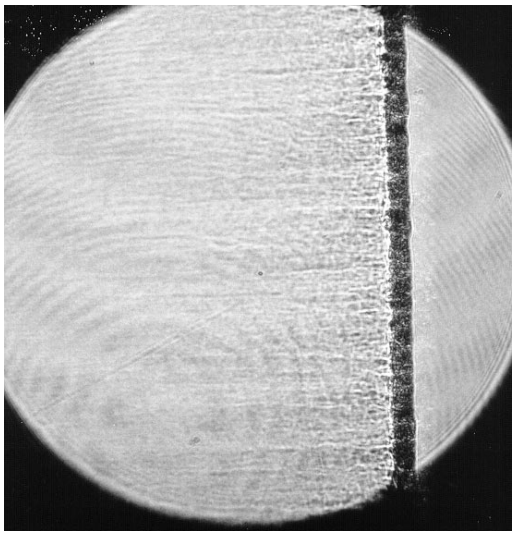

(b) Laser shadowgraph
($H_2 + 0.5O_2$, P_1 = 20 kPa)

Fig. 1 One-dimensional detonation wave.

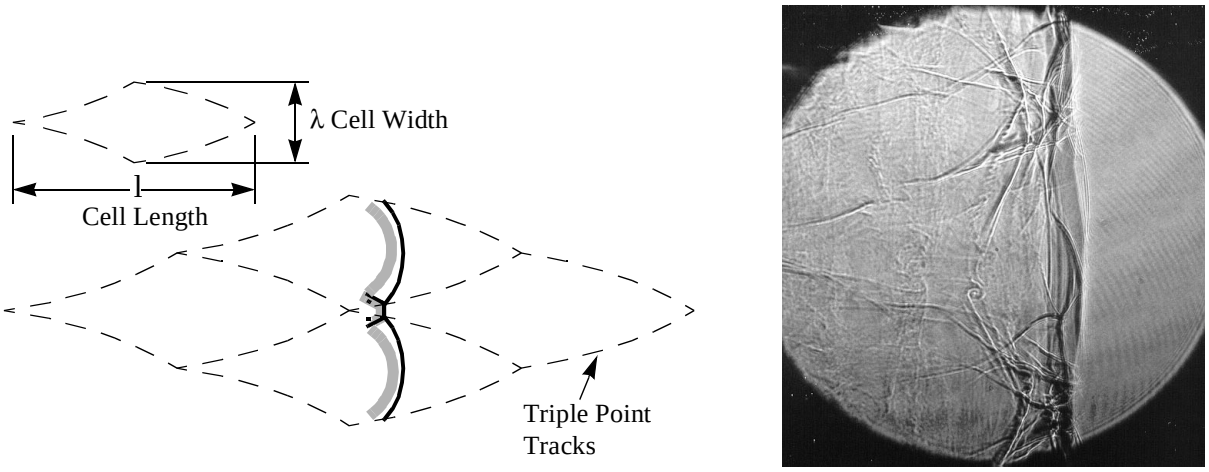

(a) Schematic of wavefront and cellular structure.

(b) Laser shadowgraph ($H_2 + 0.5O_2 + 10Ar$, P_1 = 20 kPa).

Fig. 2 Multi-dimensional detonation wave.

A detonation may form via direct initiation or deflagration to detonation transition (DDT) (Lee 1977, Shepherd 1992). The former mode is dependent upon an ignition source driving a blast wave of sufficient strength, while the latter begins with a deflagration which is able to accelerate through interactions with its surroundings to a detonation. Direct initiation by a concentrated source requires an extremely large energy deposition relative to deflagrative ignition. A deflagration can be ignited in a typical hydrocarbon mixture such as 1 bar stoichiometric propane-air with a 1 mJ spark, whereas direct initiation of a detonation in the same mixture requires over 100 kJ. This six order of magnitude difference reflects the general difficulty associated with direct initiation. On the other hand, after a small spark has created a deflagration the transition process can take a relatively long distance and time.

The present investigation represents an initial effort to understand the propagation of detonations through area changes (diffraction) and mixture composition gradients. Area changes and mixture gradients within detonation-based propulsion cycles exist due to various initiator techniques, nozzles geometries, and combustion chamber mixing constraints. These two areas of study in detonation physics are also important to the safety and scientific communities. Hazard analyses often involve the determination of whether or not a detonation can expand into an unconfined space, from a fuel line into a tank for example, and mixture gradients are invariably encountered when the fuel-air ratio is spatially varying, such as during a gas leak. The scientific study of detonations is extremely challenging due to the short time and length scales involved along with the high pressures and temperatures associated with the phenomenon. Therefore, investigative techniques typically involve macroscopically perturbing the wave, for example via a change in confinement or mixture composition, to learn about the nature of the detonation based on how it responds. This report is intended to provide some background information on the problems of detonation transmission through an abrupt area expansion and across a mixture gradient, serve to document an initial experimental effort, outline some analytical considerations, and suggest directions for the future.

1.1 Detonation Diffraction

The outcome of a detonation wave propagating from a confined to an unconfined volume through an abrupt area change will fall into one of two regimes, depending primarily on the combustible gas composition, initial thermodynamic conditions, and geometry of the confining area. The detonation is able to successfully transit the area change in the super-critical regime. Sudden expansion from confinement results in shock wave separation from the reaction zone and complete failure of the detonation wave in the sub-critical regime. Partial failure of the diffracting wave, followed by re-initiation leading to the detonation propagating throughout the unconfined volume occurs in the critical case.

Fixing all of the initial conditions except for the size of the diffraction tube leads to the so-called critical diameter experiment. As indicated in Fig. 3, a tube diameter greater than the critical diameter (d_c) results in a super-critical diffraction, a tube diameter equal to the critical diameter results in a critical diffraction, and a tube diameter less than the critical diameter results in a sub-critical diffraction. Historically, the effort on the problem of detonation diffraction consists of critical tube diameter experiments in circular tubes with the primary application of hazard analysis. Other geometries have been studied; Edwards (1979, 1981) and Thomas (1986) performed diffraction experiments in rectangular cross section channels and Thomas emphasized the effect of wall support on a detonation by varying the divergence angle of the diffraction. The work of Moen (1986) demonstrated a promotion of supercritical diffractions through an annular slot versus a circular tube.

Critical diameter data from Guirao (1982), Knystautas (1982), Makris (1994), Matsui (1979), Moen (1981, 1982, 1984, 1985), Rinnan (1982), and Zeldovich (1956) are presented in Fig. 4 for ethylene, propane, and hydrogen fuels in oxygen and with nitrogen dilution. In general, slightly fuel-rich conditions, increased initial pressure, and decreased diluent concentrations result in the smallest critical diameters. Ethylene, propane, and hydrogen is the order of fuel sensitivity in oxygen from smallest to largest critical diameters. This order changes as the mixtures are diluted with nitrogen, and becomes hydrogen, ethylene, and propane in the fuel-air case.

Knystautas (1982) provides substantial evidence that the critical diameters for these systems can be well correlated with the detonation cell width by the empirical expression of $d_c = 13\lambda$. Diffraction of overdriven detonations in similar mixtures was studied by Desbordes

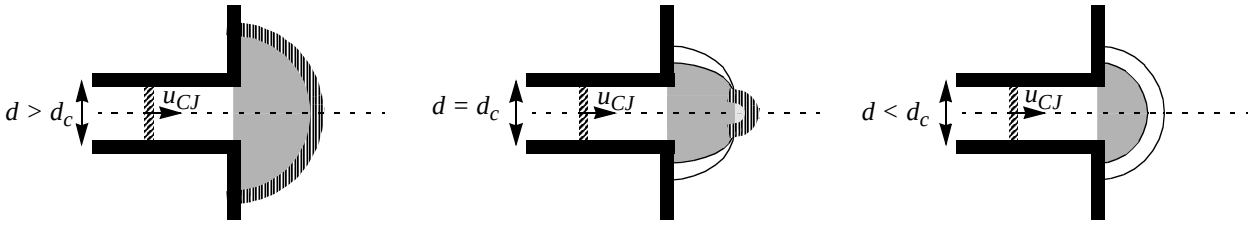

(a) Supercritical: continuous transmission without failure.

(b) Critical: partial failure followed by re-initiation.

(c) Subcritical: complete failure as shock decouples from reaction zone.

Fig. 3 Three regimes of detonation diffraction.

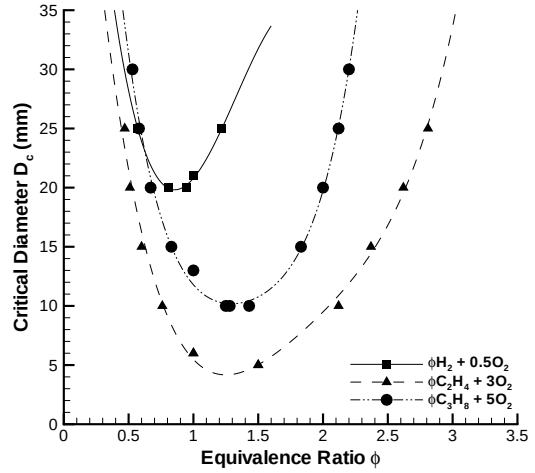

(a) Fuel-oxygen data.

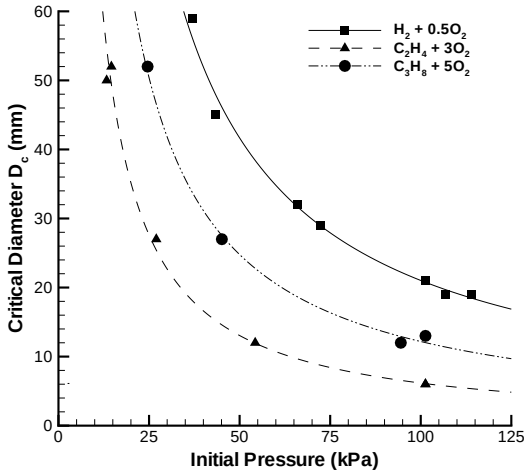

(b) Fuel-oxygen data.

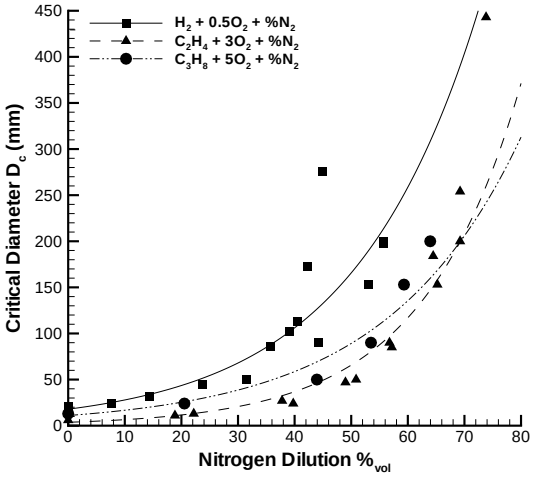

(c) Fuel-oxygen-nitrogen data.

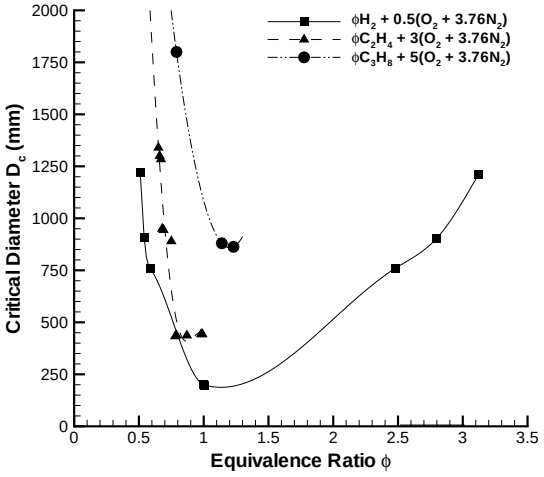

(d) Fuel-air data.

Fig. 4 Critical tube diameter data from the literature.

(1986), who found that the 13λ correlation held with λ measured in the overdriven state. However, Desbordes (1993), Moen (1986), and Shepherd (1986) conducted experiments in which various fuel-oxygen systems were diluted with monatomic gases (helium, argon, and krypton) and found that d_c varied between 4λ and 30λ depending on the type and amount of diluent. The larger critical diameters were obtained with increasing diluent concentration. Limited visualization of the diffraction process with streak and schlieren photographs has been conducted by Zeldovich (1956), Soloukhin (1969), and Edwards (1979), the latter of which found that re-initiation at critical conditions occurred via localized explosions near the head of the diffracting detonation. Des-

bordes (1986), Edwards (1979), and Thomas (1986) have recorded soot foil measurements of triple point paths during detonation diffraction.

Work-done concepts have been used by Lee (1977) and Urtiew (1981) to arrive at formulas for transforming critical diameter measurements into equivalent critical energies for direct detonation initiation. Edwards (1979, 1981) presents a criterion for calculation of the critical diameter based on an assumed critical velocity gradient equated to the velocity gradient existing in a two-dimensional non-reacting shock diffraction as given by Whitham (1957). His results are in accord with approximately two-dimensional experiments, but as with the empirical correlations, use of the criterion requires knowledge of the detonation cell width. Stability parameters calculated with empirical chemical induction time expressions by Moen (1986) and detailed chemical kinetics computations by Shepherd (1986) have attempted to shed light on the breakdown of the 13λ correlation for monatomically diluted mixtures. Murray (1986) discusses the critical diameter problem in terms of stream tube divergence issues highlighted in his work with detonations propagating under conditions of yielding confinement. Plausible explanations for observed detonation diffraction phenomena were obtained by all of these researchers, but little in the way of conclusive evidence and correlation has been identified.

A recent overview paper by Lee (1996) summarized the understanding of the relationship between the critical tube diameter and detonation cell width through some of the work of the aforementioned researchers and his own thoughts. The mixtures for which the 13λ correlation seems to hold tend to have irregular cellular structure (cell width measurements vary by $\pm 50\%$), high chemical activation energies, and detonation initiation is marked by localized explosions. Extreme temperature sensitivity is characteristic of these mixtures, and so it might be expected that the expansion of a diffracting detonation near criticality results in immediate decoupling of the shock from the reaction zone. The problem of re-initiation then becomes chemistry independent, so that similar gas- and thermodynamic conditions present in these mixtures leading to the formation of localized explosions for re-initiation result in the nearly universal correlation. On the other hand, mixtures with high concentrations of monatomic diluents generally exhibit very regular cellular structure, have low activation energies, and observations provide a picture of uniform detonation initiation rather than explosion of discrete sites. Lee speculates that due to the decreased temperature sensitivity of these mixtures, a more gradual failure occurs which is linked to a critical curvature of the diffracting detonation front. Lee concisely points out the fundamental problem of detonation diffraction research: “Currently there is no general theory for the prediction of the critical diameter.”

1.2 Detonation Transmission Through a Mixture Gradient

The gradient transmission problem is that of a detonation moving from one mixture into another, either through a discontinuous change in mixture or a continuous mixture variation. A detonation propagating from a more to less sensitive mixture can continuously adjust and travel as a CJ wave corresponding to the local conditions, fail and then re-initiate, or fail completely. Note the similarity to the supercritical, critical, and subcritical phenomena of detonation diffraction. A simple model of a detonation impinging on a contact surface formed by the boundary between two mixtures is an extension of a non-reacting shock interaction with a contact surface. As illustrated in Fig. 5, the incident shock (I) causes a shock wave (T) to be transmitted across the contact

surface (CS), and either a shock (R_{shk}) or expansion (R_{exp}) is reflected from the contact surface. The strength of the transmitted wave and the type and strength of the reflected wave is dictated by the initial conditions and matching of the pressure and fluid velocity across the contact surface between the transmitted and reflected waves.

Paterson (1953) performed an analysis of a detonation impinging on a contact surface between a combustible and inert mixture using the model presented above. He took the gas state behind the incident wave as the CJ conditions of the detonation wave (i.e., infinite kinetic rates), arguing that the conditions during the induction period existed for such a short time as to be inconsequential. Paterson also noted that his assumption of a continuous region behind the wave at CJ conditions is not realistic (neglecting the following Taylor expansion wave), but expected this to be valid for calculating the initial transmitted shock strength. The analysis was extended to combustible mixtures on both sides of the contact surface by introducing an ad hoc one parameter characterization of the degree of reaction in the receptor mixture.

Thomas (1991) used Paterson's non-reacting receptor analysis and found excellent agreement with the initial strength of the transmitted shock when compared to experiments in which a detonation impinged on an inert contact surface. The experimental observations were of an initially decaying transmitted shock which levelled off a short time after the contact surface interaction. This decay to a plateau value was accurately captured by Thomas with computations taking the Taylor expansion following the detonation wave into account. Experiments in which the contact surface was allowed time to diffuse demonstrated the detonation wave velocity and cellular structure rapidly conforming to the local mixture conditions.

Bjerketvedt (1986), Bull (1981), Engebretsen (1993), and Thomas (1991) have studied the transmission of detonations across an air gap between combustible mixtures, often determining critical air gap lengths and time/distance for re-initiation once the transmitted shock entered the second combustible mixture. The second mixture was always the same as the first or less sensi-

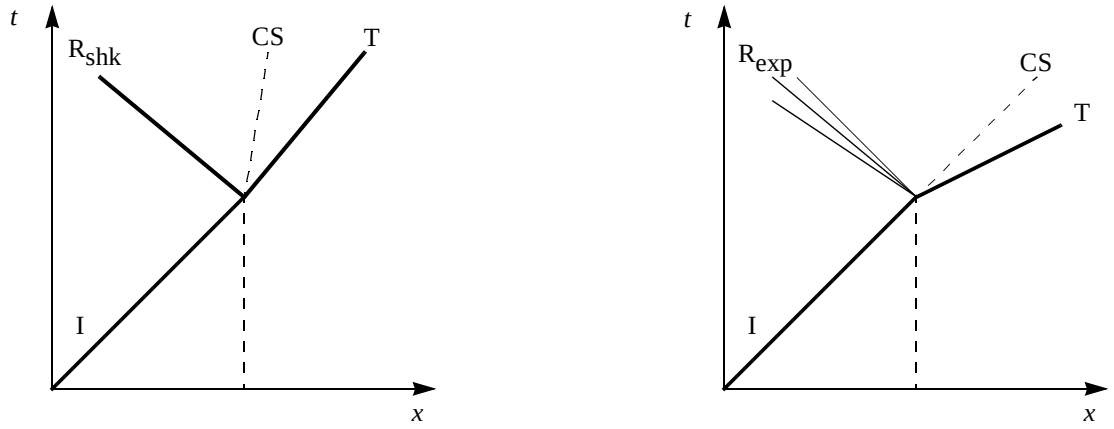

(a) Reflected shock case. (b) Reflected expansion case.

Fig. 5 Time-distance diagrams of possible shock-contact surface interactions.

tive, and the re-initiation process was generally found to exhibit DDT characteristics. Bull's study used the Brinkley-Kirkwood (1947) blast decay theory to approximate the transmitted shock trajectory through the air gap. Thomas showed that gradual gradients significantly assist the transmission process, whereas sharp gradients tend to cause immediate decoupling of the shock and reaction zone.

Engebretsen (1993) and Strehlow (1972) have conducted experiments of detonation transmission through combustible mixture gradients, with the former focusing on identifying conditions under which the detonation could continue to propagate and the latter investigating the effect of mixture perturbation on the detonation cellular structure. Strehlow applied his theory for determining the strength of transverse waves, and found that the transverse wave systems adapt much more quickly when a detonation is propagating from low to high sensitivity regions. He also noted that the transverse waves persist for a long distance beyond an interface with inert gas, with an average decay rate of 7% per cell length.

Many of the experiments mentioned above were performed in vertical tubes with density gradients to assist in the formation of stable contact surfaces. Fast-acting slider valves were used to separate the mixtures during the fill process, and Bjerketvedt (1986) and Engebretsen (1993) conducted mixing/diffusion experiments on the mixture interface after the valve was opened. Bjerketvedt indicates that after 250 msec, a mixing zone of less than 30 mm existed for a 100 msec slide valve opening time. Engebretsen found a mixing region approximately 60 mm long after 250 msec.

2 Documentation of Diffraction Regimes

The first series of experiments were conducted with a 280 mm detonation tube coupled to a test section via a small diameter tube to obtain visual and velocity/pressure history documentation of the aforementioned possible outcomes of detonation diffraction.

2.1 Experimental Procedure

The 280 mm diameter stainless steel detonation tube is 7.3 m long with a 25 mm wall thickness. The 762 mm long, 152 mm square stainless steel test section is mated to the end of the detonation tube. A 610 mm long, 25 mm diameter aluminum tube is sandwiched between the detonation tube and test section so that one end protrudes into the 165 mm diameter test section window. The experimental configuration is illustrated in Fig. 6.

Prior to an experiment the entire assembly is evacuated to a pressure level below 7 Pa, and then the desired gas mixture composition is filled via the partial pressure technique. The concentration accuracy of each mixture constituent is limited to the electronic Heise 901a gauge accuracy of ±0.18 kPa. After filling, the mixture is circulated through the tubes and test section for 5 min to ensure mixture homogeneity. The ignition system utilizes an oxygen-acetylene driver, injected into the end of the detonation tube where a 30 mm long copper wire is located. The copper wire is exploded through a 2 μF, 9 kV capacitor discharge which causes direct initiation of the driver gas. The driver detonation, with an equivalent energy of approximately 50 kJ, transmits a

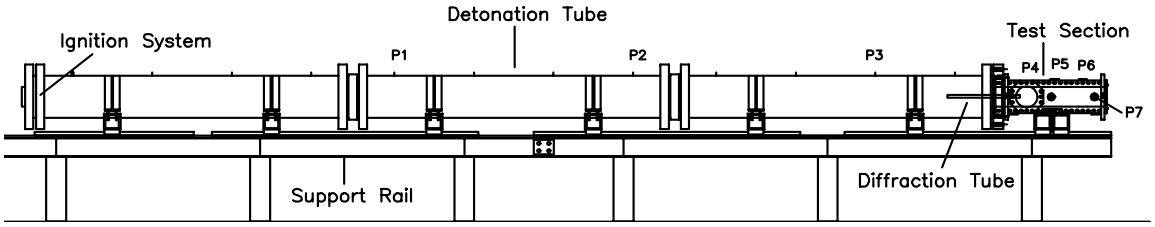

(a) Detonation tube schematic.

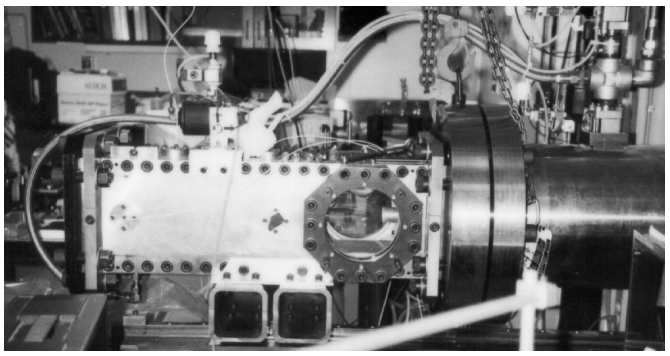

(b) Test section with diffraction tube installed.

Fig. 6 Experimental configuration.

detonation into the test mixture. Piezoelectric pressure transducers located in the detonation tube and test section walls recorded shock wave time-of-arrival and pressure data. A ruby laser shadowgraph system, shown in Fig. 7, was used to image the diffraction of detonations from the small tube into the test section. The Chapman-Jouguet detonation velocity V_{CJ} is calculated with the thermochemical equilibrium computer code STANJAN (Reynolds 1986).

2.2 Results

Table 1 contains a summary of the conditions investigated. The outcome of an experiment, either sub-critical, re-initiating, or super-critical, indicates whether or not the detonation was able to successfully diffract through the area change and is discussed further below. Note that the following sequences of shadowgraphs illustrating the evolution of each regime are from different experiments under the same conditions, and the images are integrated across the flowfield in the test section window. The rectangle at the top of the diffraction tube in the images is a 1 cm long scale. Some of the pressure traces decay below zero after passage of the detonation wave, indicative of thermal effects on the transducer.

Ruby laser shadowgraphs representative of the super-critical case are presented in Fig. 8. The detonation is able to continuously transit the area change without failure. Pressure data from a super-critical diffraction experiment are presented in Fig. 9. The reflected shock from the detonation tube end wall is clearly visible in the third pressure trace, as are the reflected shocks inside of the test section in the final four traces. Note that the pressure amplitude from transducer six was lower than expected during all of the experiments, indicating a recalibration is necessary. The spike in the last two pressure traces just prior to the arrival of the detonation wave is a result of the capacitor discharge through the ruby laser flashlamp.

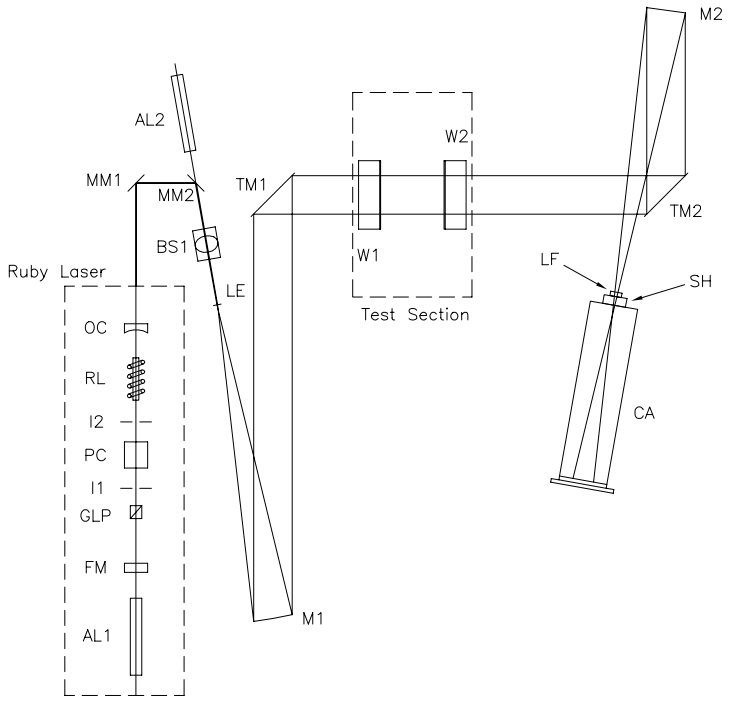

AL1	He-Ne Alignment Laser
FM	Rear Cavity Mirror
GLP	Glan Laser Polarizing Beam Splitter
I1	Iris
PC	Pockels Cell
I2	Iris
RL	Ruby Rod & Flashlamp
OC	Output Coupler
MM1	Turning Mirror
MM2	Turning Mirror
AL2	He-Ne Alignment Laser
BS1	Beam Stearing Mirror Pair
LE	Beam Expanding Lens
M1	Concave Mirror
TM1	Input Turning Mirror
W1	Input Test Section Window
W2	Output Test Section Window
TM2	Output Turning Mirror
M2	Concave Mirror
LF	Laser Line Filter
SH	Capping Shutter
CA	Camera Box (with 4”x5” back)

Fig. 7 Ruby laser shadowgraph layout.

Table 1: Diffraction regime documentation experimental conditions.

Gas Mixture	Initial Pressure (kPa)	Velocity V_{CJ} (m/s)	Cell Width λ (mm)	Transmission Regime
$2H_2+O_2$	100	2841	1.4	Critical
	90	2836	1.6	Critical
	85	2832	1.7	Critical
	80	2829	1.9	Sub-Critical
	70	2822	2	Sub-Critical
$2H_2+O_2+3.76N_2$	100	1971	15.5	Sub-Critical
$C_2H_2+2.5O_2$	30	2358	1	Super-Critical
	20	2337	1.5	Super-Critical
	10	2300	2	Super-Critical
	5	2264	4	Super-Critical
$C_2H_2+2.5O_2+14Ar$	90	1711	1.4	Sub-Critical
	70	1703	1.8	Sub-Critical
	50	1691	3	Sub-Critical

The sudden expansion from the confinement of the small tube results in complete failure of the detonation wave in the sub-critical regime. As shown in Fig. 10, the shock wave separates from the reaction zone and rapidly decelerates. Pressure data from a sub-critical diffraction experiment are presented in Fig. 11. It is not clear whether the contact surface is a deflagration or the expansion has completed quenched the reactions. The non-detonative lead shock of the final three pressure traces reflects from the test section end wall and forms a detonation propagating back towards the diffraction tube. Note that the experiment shown had a bad signal from pressure transducer six, and therefore its data trace has been omitted.

Near-critical conditions are characterized by partial failure of the diffracting wave, followed by re-initiation leading to the detonation propagating throughout the unconfined volume. The shadowgraphs of Fig. 12 contain a re-initiation in progress. Localized explosions occur between the shocked reactants and that portion of the detonation not yet affected by the expansion to begin the re-initiation process (Fig. 12b). The blast waves and energy release from these discrete sites couple into a detonation front propagating spherically outward and sweeping back into the shocked reactants (Fig. 12c,d). The highly non-uniform flowfield is a result of the random, stochastic nature of explosion center formation. Pressure data from a critical diffraction experiment are presented in Fig. 13. The shock reflections are evident as in the other experiments, and the amplitude from pressure transducer six is low as mentioned above.

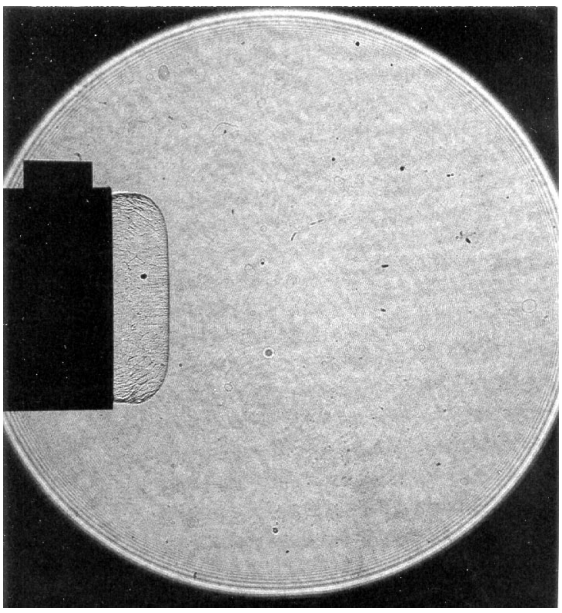

(a) 3177 μsec, Shot 510

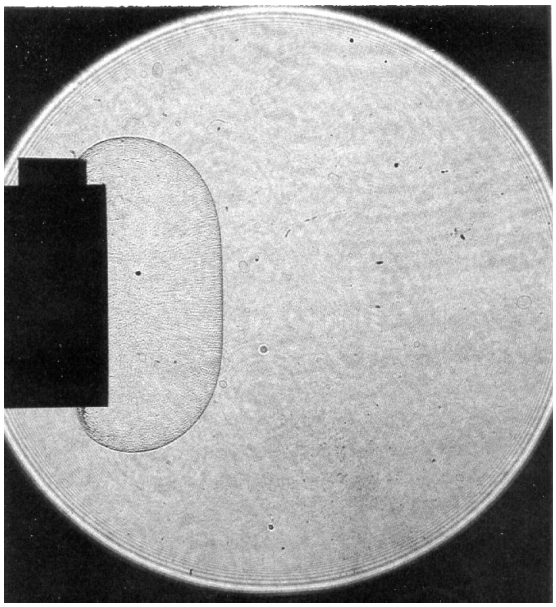

(b) 3181 μsec, Shot 509

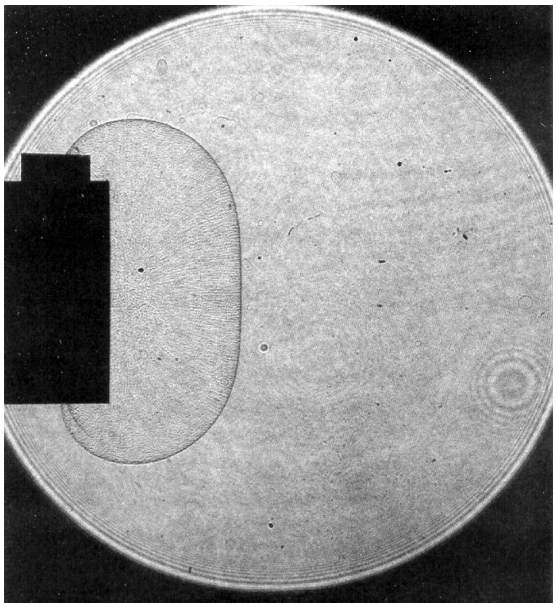

(c) 3185 μsec, Shot 508

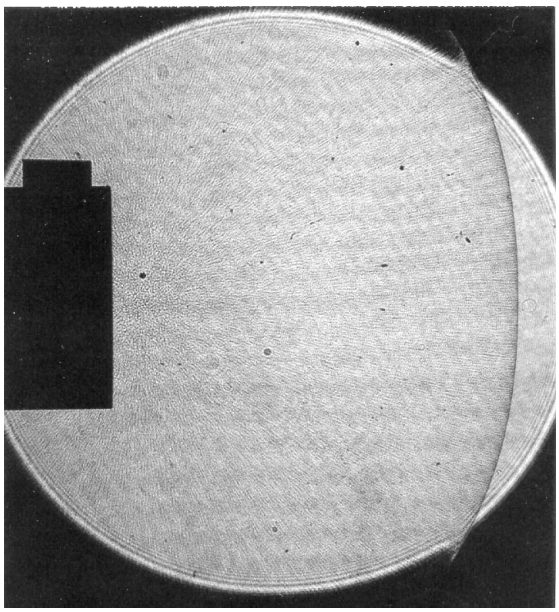

(d) 3200 μsec, Shot 511

Fig. 8 Shadowgraphs of super-critical detonation diffraction in 30 kPa C_2H_2+2.5O_2.

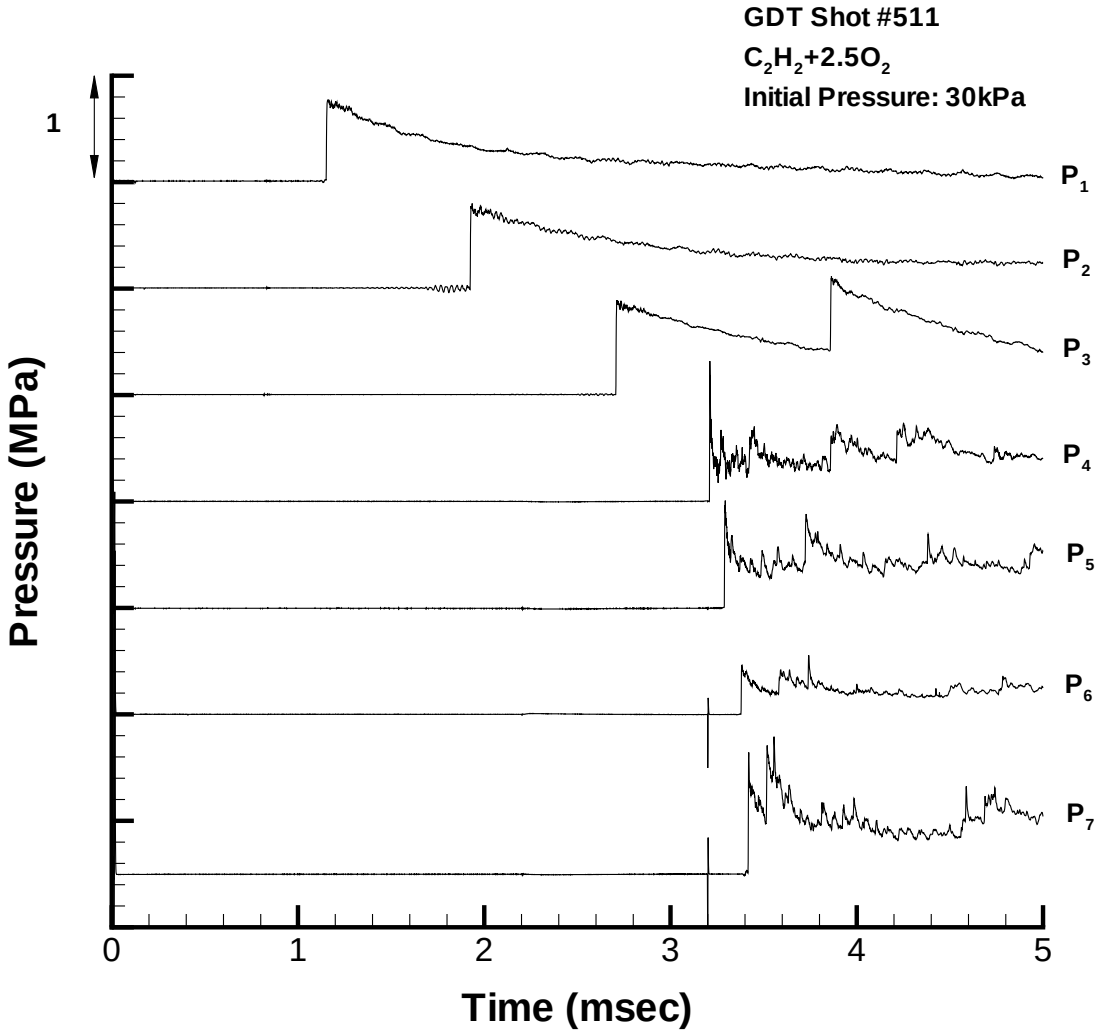

Fig. 9 Pressure versus time data for super-critical detonation diffraction.

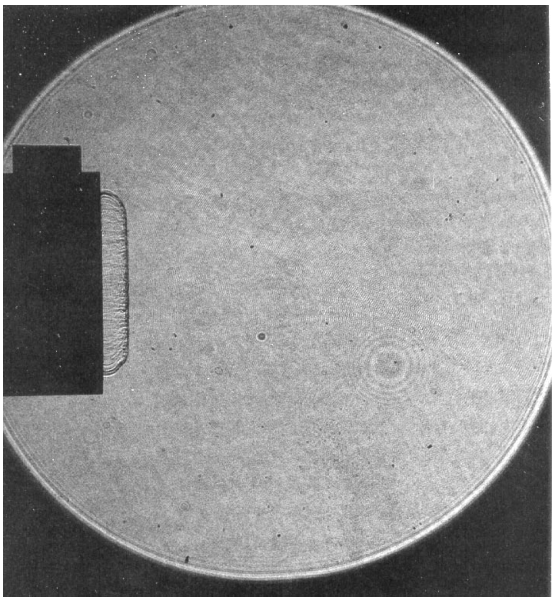

(a) 2656 μsec, Shot 497

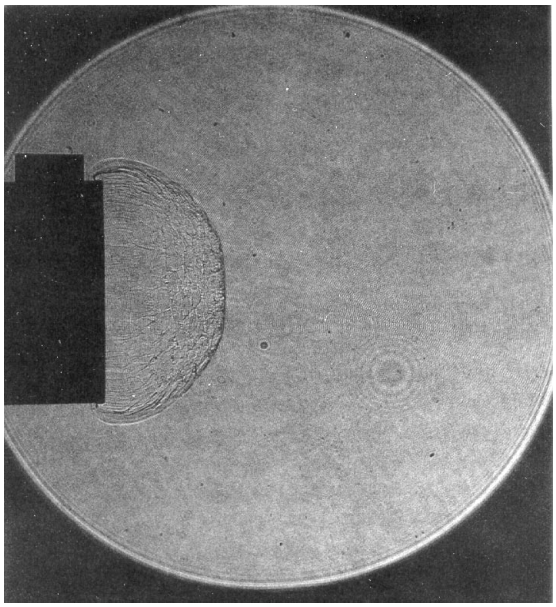

(b) 2660 μsec, Shot 496

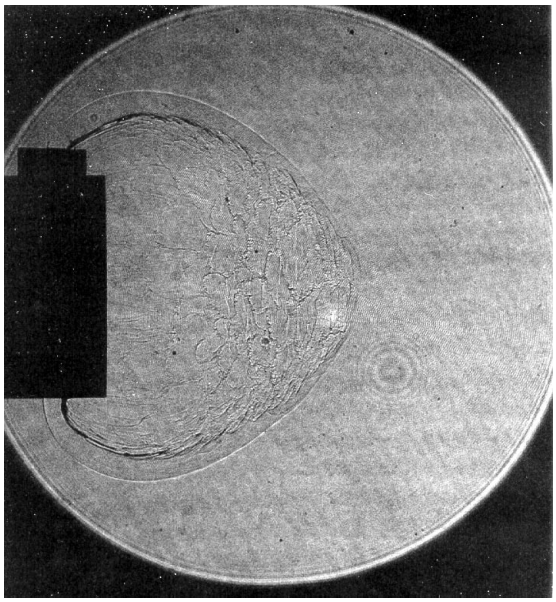

(c) 2670 μsec, Shot 495

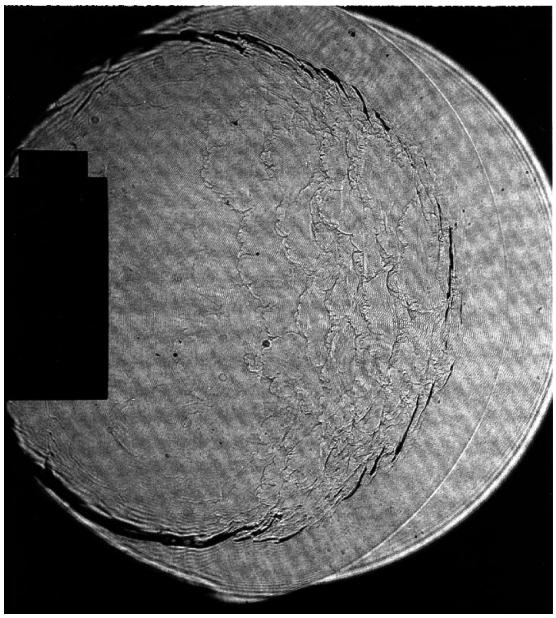

(d) 2690 μsec, Shot 494

Fig. 10 Shadowgraphs of sub-critical detonation diffraction in 70 kPa $2H_2+O_2$.

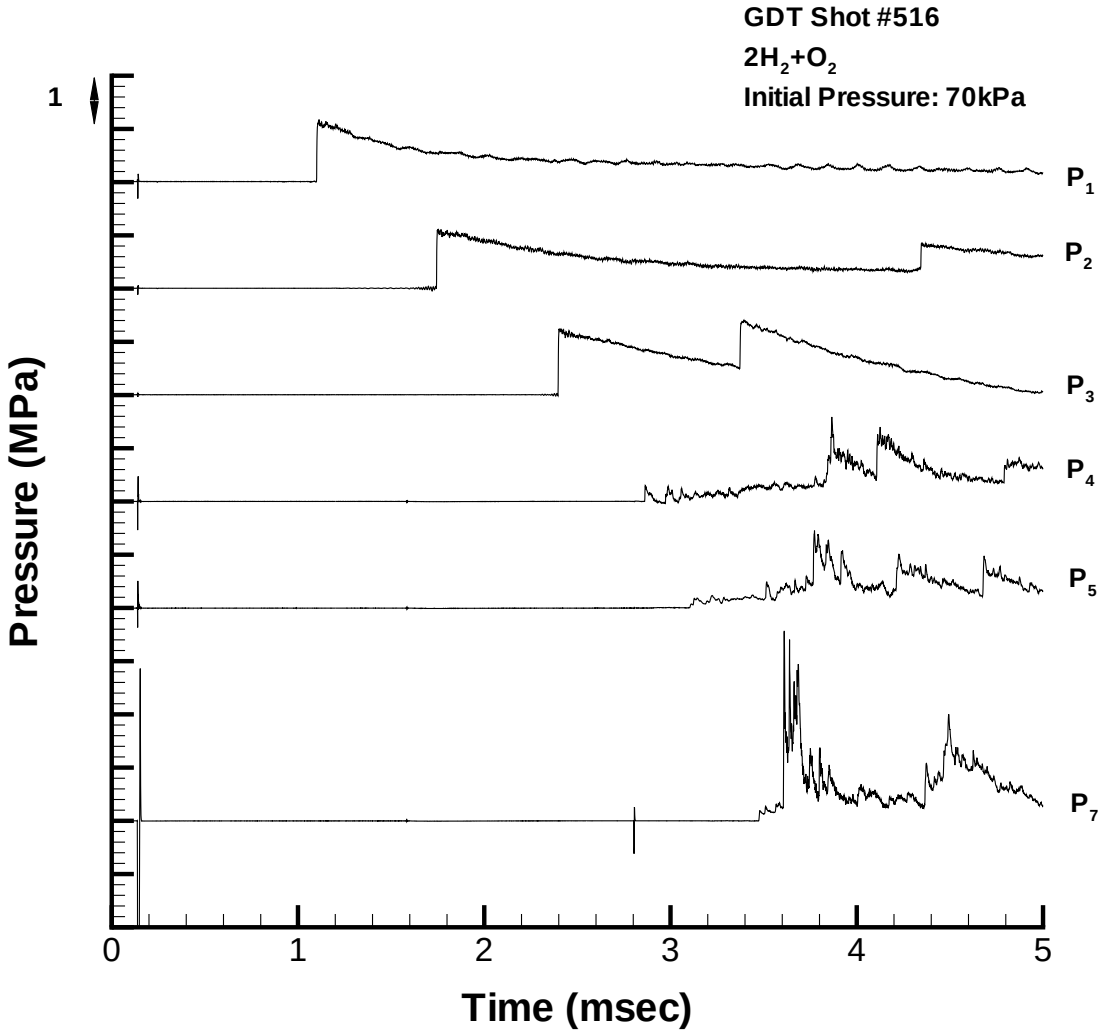

Fig. 11 Pressure versus time data for sub-critical detonation diffraction.

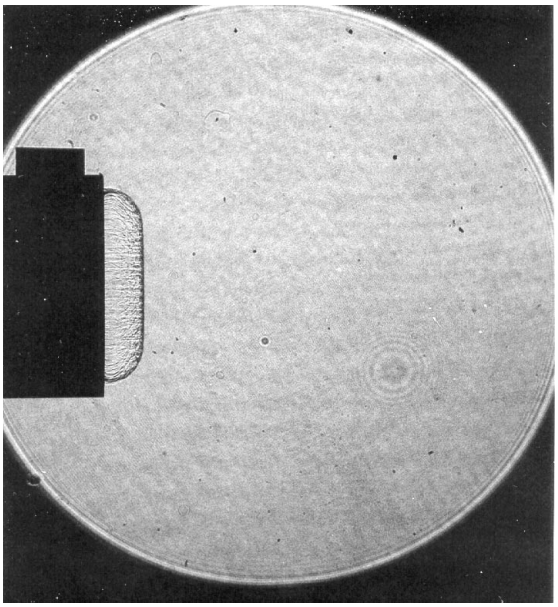

(a) 2635 μsec, Shot 500

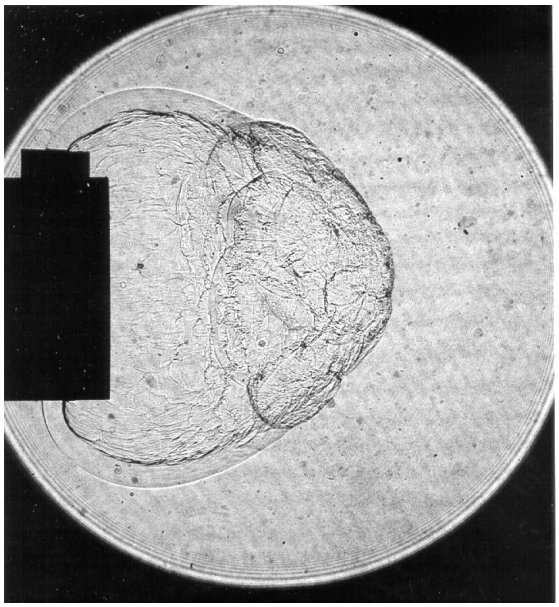

(b) 2649 μsec, Shot 520

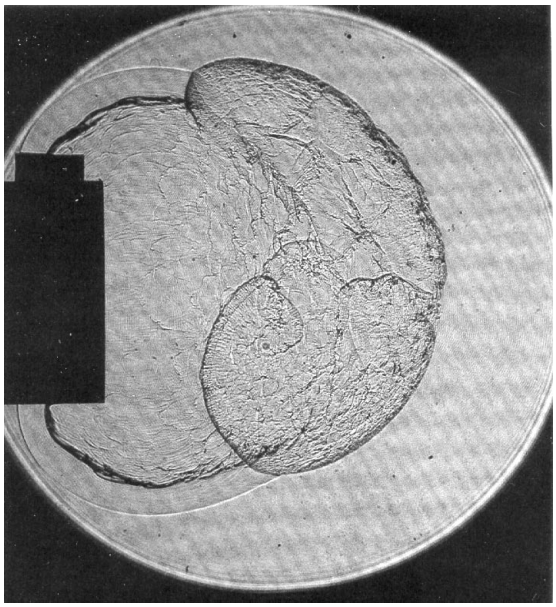

(c) 2650 μsec, Shot 498

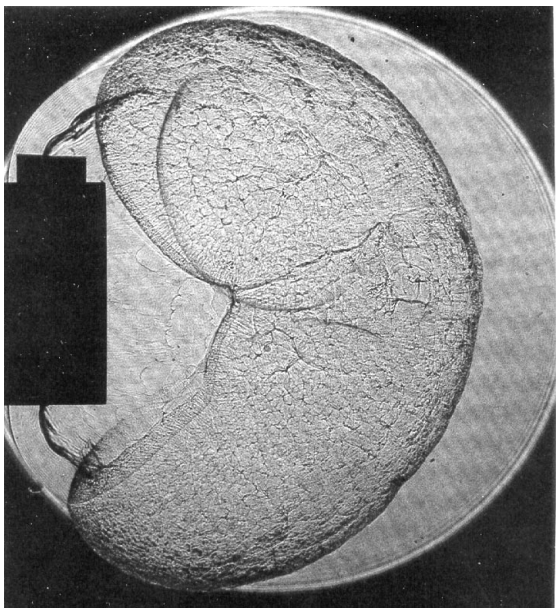

(d) 2655 μsec, Shot 502

Fig. 12 Shadowgraphs of critical detonation diffraction in 100 kPa $2H_2+O_2$.

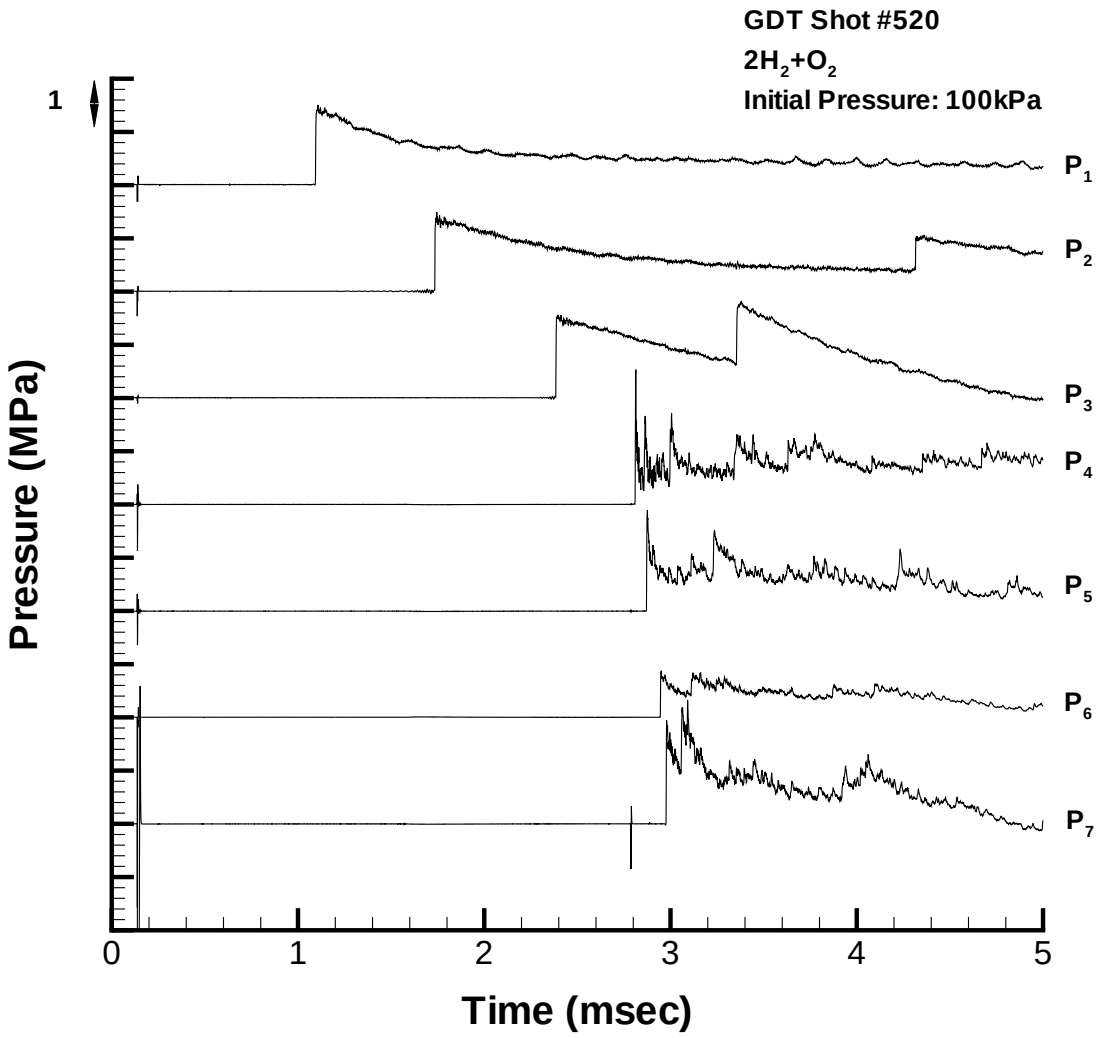

Fig. 13 Pressure versus time data for critical detonation diffraction.

3 Investigation of Critical Diffraction Limits

Experiments were conducted in a different experimental facility with 1 bar stoichiometric hydrogen, ethylene, and propane fuel mixtures of variable nitrogen dilution to determine the critical conditions for detonation diffraction.

3.1 Experimental Procedure

A diffraction tube was designed and fabricated for use with the test section discussed previously. The 38 mm diameter, 2024-T3 aluminum tube is 1.5 m long and mounts as shown in Fig. 14, with 67 mm between the tube end and the center of the test section window. The ignition source consists of a spark plug mounted in a Teflon end cap, followed by a turbulence-inducing spiral which enhances transition of the spark-induced deflagration to a detonation. Three instrument mounts are located along the length of the tube, spaced 40 cm apart. These mounts hold pressure transducers for monitoring the velocity and pressure profile of the detonation wave, and plumbing for the gas handling (fill and evacuation) system. Provisions for a diaphragm or air cylinder-driven gate valve (<0.4 sec opening time) are located at the end of the tube for separating the diffraction tube mixture from the test section mixture. The diaphragm or gate valve location is 8 mm from end of the diffraction tube. The tube and all fixtures include o-ring seals to maintain vacuum and mixture integrity. The entire assembly was designed to withstand four times the maximum expected dynamic pressure of 100 bar, with even greater factor of safety in many components.

A detonation wave propagating at 2000 m/s will transit the 40 cm distance between pressure transducers in 200 μsec. The transducers have a 1 μsec rise time, and so the typical time-of-arrival measurement error is ±1 μsec. It is not unreasonable to assume that the measured transit time for this hypothetical detonation could be 198 μsec or 202 μsec, resulting in apparent velocities of 1980 m/s and 2020 m/s, respectively. Therefore, the relatively closely spaced pressure transducers result in a velocity measurement uncertainty of approximately ±1%.

Prior to all experiments the diffraction tube and test section were evacuated to less than 14 Pa. The mixtures investigated were comprised of either hydrogen, ethylene, or propane fuel in

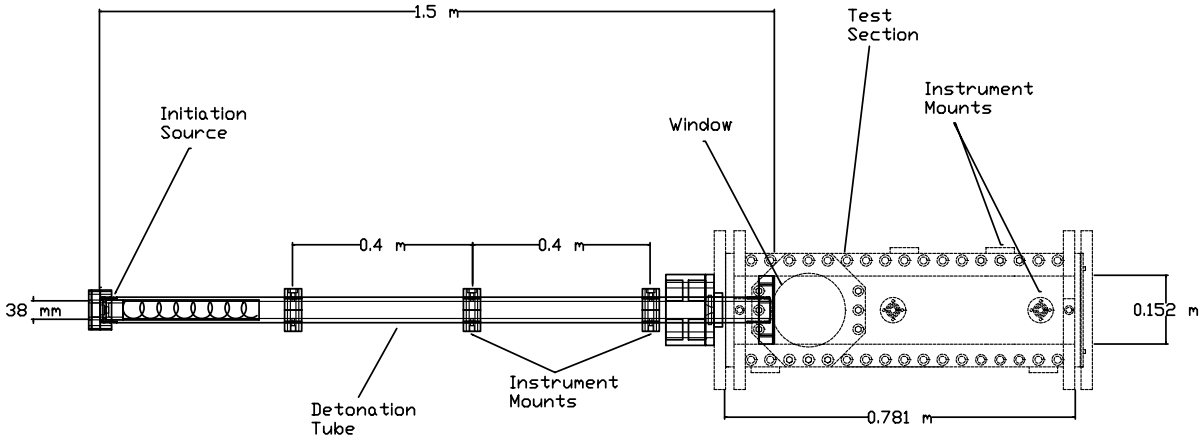

Fig. 14 Experimental apparatus for the investigation of critical diffraction limits.

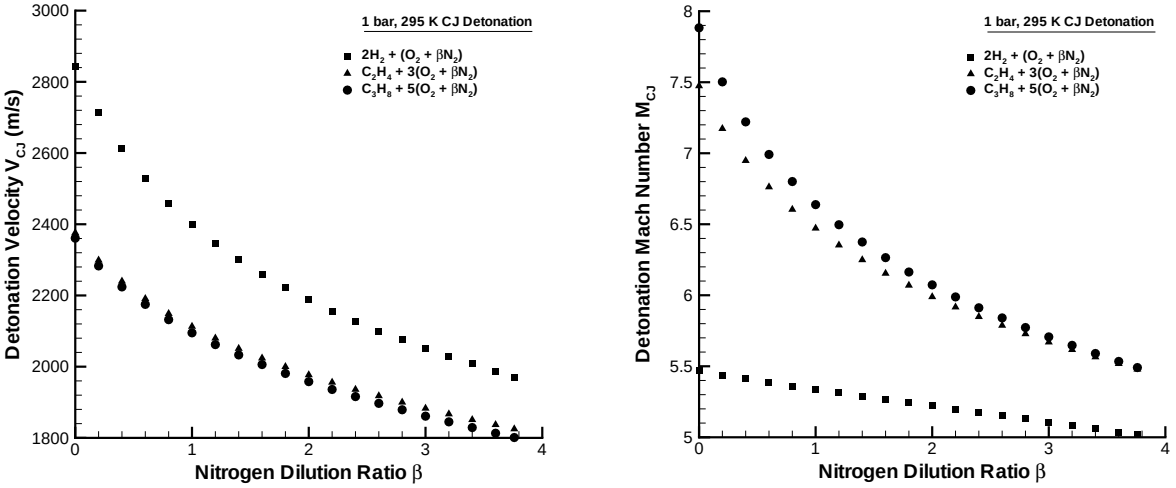

(a) Velocity.

(b) Mach number.

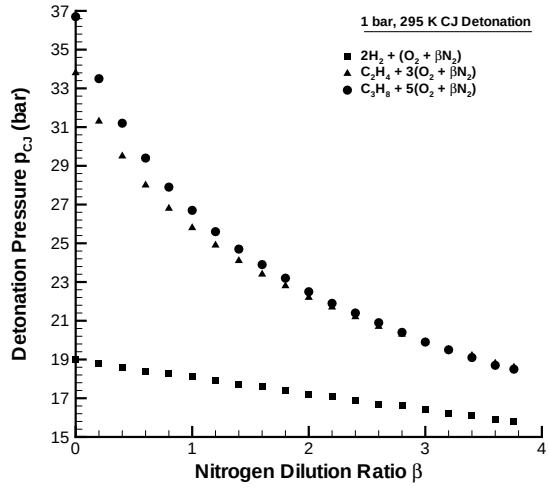

(c) Pressure.

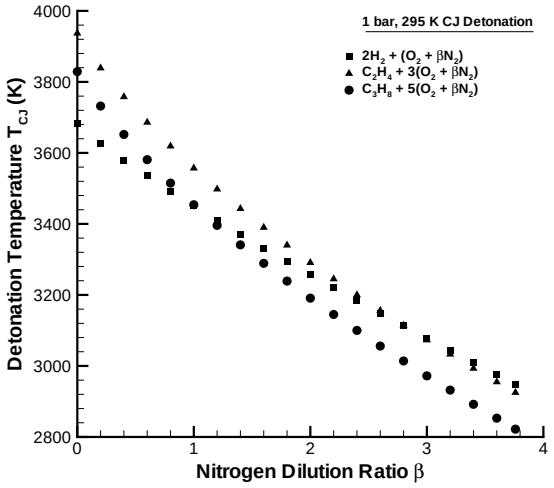

(d) Temperature.

Fig. 15 CJ detonation properties for fuel-oxygen-nitrogen mixtures.

stoichiometric proportions with oxygen (fuel equivalence ratio $\phi = 1$) and diluted with variable concentrations of nitrogen. Characteristic wave velocities, Mach numbers, pressures, and temperature associated with CJ detonations in these mixtures were calculated with STANJAN and are presented in Fig. 15. Constituent gases were filled via the partial pressure technique, and the final 1 bar, 295 K mixture was pump-circulated for 15 min to ensure homogeneity. Detonations were initiated at the end of the diffraction tube with the spark plug and spiral, which then propagated through the diffraction tube mixture towards the test section. The detonation diffracted into the test section where the window afforded flow visualization of the expansion process. Based on the first series of diffraction regime documentation experiments, pressure transducer measurements

and ruby laser shadowgraph images were used to determine whether or not the detonation was able to successfully transition into the test section mixture.

Two types of experiments were conducted:

(1) *One mixture* in which the diffraction tube was connected to the test section and both were filled with a common fuel-oxygen-nitrogen mixture. The nitrogen dilution ratio β (defined as the ratio of nitrogen to oxygen concentration, so that $\beta = 3.76$ corresponds to air) was varied until the critical diffraction regime was identified.

(2) *Two mixture* in which the diffraction tube was connected to the test section and a gate valve separated the diffraction tube fuel-oxygen mixture from the fuel-oxygen-nitrogen mixture in the test section. The gate valve was opened less than 0.4 sec prior to the spark ignition. The nitrogen concentration was varied to identify the critical β value.

3.2 Results

Appendix A and B contain data pertinent to all of the one mixture and two mixture experiments, respectively. The average detonation velocity measured in the diffraction tube between the three pressure transducers is denoted by V_{avg}, and the $\%V_{CJ}$ deficit column indicates the departure of the measured velocity from the CJ detonation velocity. Moen (1986) and Murray (1986) found that the actual detonation velocity is decreased from the CJ velocity for relatively small tube diameters relative to the detonation cell width of the mixture because of momentum and energy losses to the boundary layers at the tube wall. This phenomena is not clearly indicated by the measurements because most of these mixtures have cell widths much smaller than the 38 mm tube diameter (see Fig. 18), and highly accurate velocity measurements are complicated by the aforementioned ±1% velocity uncertainty. Confidence exists that a well-defined CJ detonation existed prior to diffraction in all experiments because the measured velocity departure from V_{CJ} was always negative or much less than 1% when positive. The 'Visualization' column indicates whether or not a ruby laser shadowgraph of the diffraction was obtained. The 'Criticality' column is either sub- or super-critical, and the critical case is defined as the midpoint in β of the two limiting cases. The critical β data for each mixture class in the one and two mixture experiments are summarized in Tables 2 and 3, respectively. In all cases the nitrogen dilution for supercritical diffraction was greater when the diffraction tube was filled with undiluted fuel-oxygen.

Table 2: Diffraction limits for one mixture experiments (P_1 = 100 kPa, T_1 = 295 K).

Mixture	Critical β	Cell Width λ (mm)
$2H_2 + (O_2 + \beta N_2)$	0.69	1.9
$C_2H_4 + 3(O_2 + \beta N_2)$	1.04	1.6
$C_3H_8 + 5(O_2 + \beta N_2)$	0.58	1.8

Table 3: Diffraction limits for two mixture experiments (P_1 = 100 kPa, T_1 = 295 K).

Diffraction Tube Mixture	Cell Width λ (mm)	Test Section Mixture	Critical β	Cell Width λ (mm)
$2H_2 + O_2$	1.1	$2H_2 + (O_2 + \beta N_2)$	1.28	2.7
$C_2H_4 + 3O_2$	0.6	$C_2H_4 + 3(O_2 + \beta N_2)$	1.30	2.1
$C_3H_8 + 5O_2$	1.6	$C_3H_8 + 5(O_2 + \beta N_2)$	0.74	3.2

The shadowgraphs for these experiments, included in Appendix C, were all similar to those presented for documentation of the diffraction regimes except for the two mixture experiments in which the hydrogen-oxygen diffraction tube detonation diffracted into the hydrogen-oxygen-nitrogen test section mixture. These mixtures have a substantial difference in molecular weight, resulting in a more dense test section mixture. When the gate valve is removed, gravity currents are induced along the contact surface separating the two mixtures. The lighter diffraction tube mixture tends to flow up and out into the test section, while the heavier test section gas flows down and into the diffraction tube. The resulting shadowgraphs depict an unsymmetric diffracting wave which has propagated further into the test section at the top than at the bottom. This observation is consistent with the greater CJ detonation velocity in the hydrogen-oxygen mixture flowing from the top of the diffraction tube into the test section. A representative shadowgraph of an unsymmetric detonation diffraction is presented in Fig. 16.

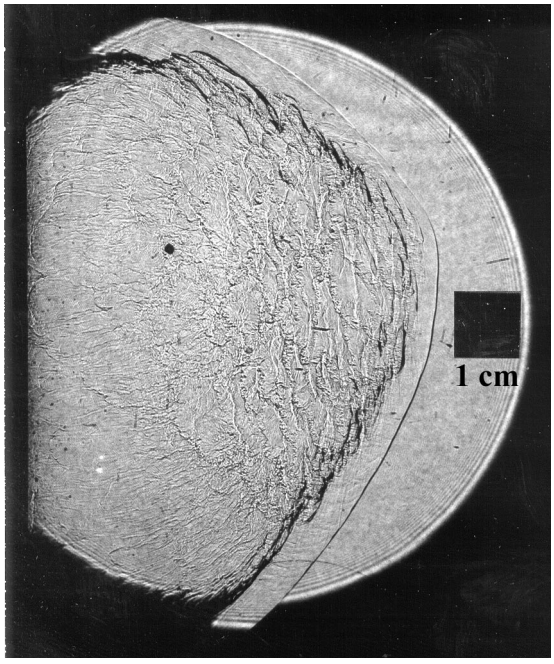

Fig. 16 Shadowgraph of subcritical unsymmetric diffraction from $2H_2 + O_2$ into $2H_2 + O_2 + 1.3N_2$, Shot 749.

4 Measurement of Cellular Structure

The final series of experiments was aimed at measuring the detonation cell width of mixtures used in the diffraction experiments to assist in analysis of the results.

4.1 Experimental Procedure

The 280 mm diameter detonation tube used for the diffraction regime documentation experiments was used for the cellular structure experiments, with an end flange installed instead of the diffraction tube and test section. A soot-covered rectangular 64 x 91.4 x 0.5 mm aluminum sheet is rolled into a cylinder to conform to the internal tube surface. This so-called soot foil is anchored inside of the tube just ahead of the end flange for the detonation to propagate over it. The triple points of the detonation front and associated sliplines form high shear regions which leave the triple point trajectories scoured in the soot. Approximately 10 - 20 cell widths are measured manually for each experiment, from which minimum, maximum, and average cell widths are generated corresponding to the initial conditions of the particular experiment. Cell width measurements are complicated by the three-dimensionality of the detonation front recorded on a two-dimensional soot foil, manual interpretation, and irregularity of the cellular structure itself. Experience in this laboratory has shown that a useful rule of thumb for most cell width data is that the minimum and maximum are given by the average ±50%. Many of the ethylene and propane experiments were conducted at subatmospheric pressure to remain under a 50 bar reflected shock safety limit of the detonation tube. These mixtures were used for at least two subatmospheric experiments in which the initial pressure was varied to obtain a measure of confidence in extrapolation of the cell width data to 1 bar.

4.2 Results

Appendix D contains pertinent data from the cellular structure experiments in tabulated form. Representative soot foils for stoichiometric propane-oxygen-nitrogen detonations are presented in Fig. 17. Increasing initial pressure with all other conditions held constant results in decreasing cell width, as illustrated in Figs. 23a and 23b. A comparison of Figs. 23a and 23c demonstrates that greater nitrogen concentration increases the cell width. The cellular structure of a 1 bar propane-air detonation is shown in Fig. 23d. Irregularity and substructure within cells are evident in all of these nitrogen diluted mixtures.

Cell width data for 1 bar initial pressure is plotted in Fig. 18. All of the hydrogen data, the ethylene-air data, and the propane-air data were directly measured at 1 bar, while the ethylene and propane data for $\beta < 3.76$ was extrapolated from subatmospheric pressure experiments. Linear extrapolations between two measurements are in good agreement with cell width dependence on the inverse of the initial pressure ($\lambda \sim P^{-1}$) expected from dimensional analysis considerations. In addition, these extrapolated values were checked with success against cell width data published in the literature.

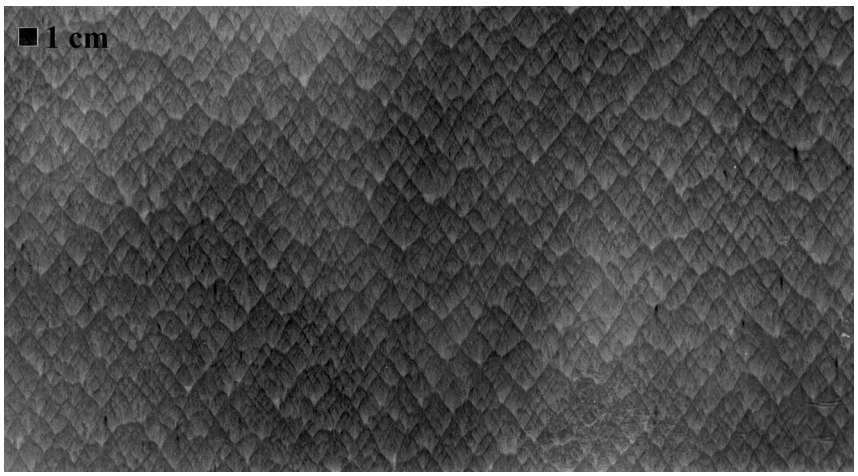

(a) β = 1, 30 kPa, Shot 909.

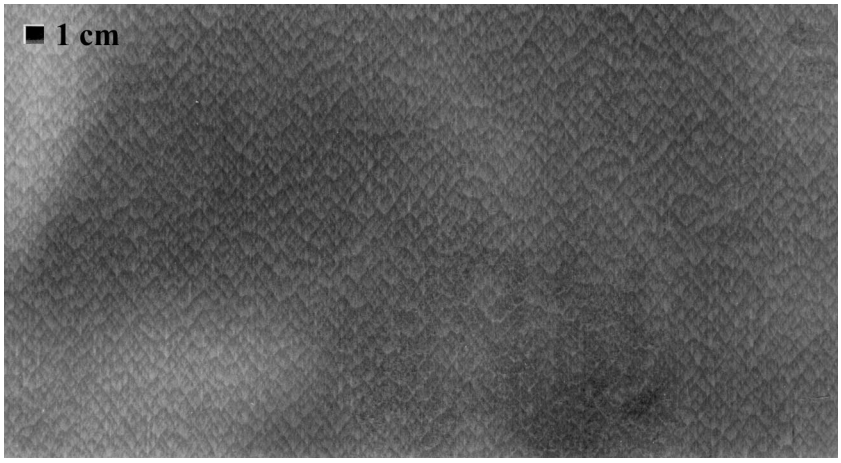

(b) β = 1, 70 kPa, Shot 912.

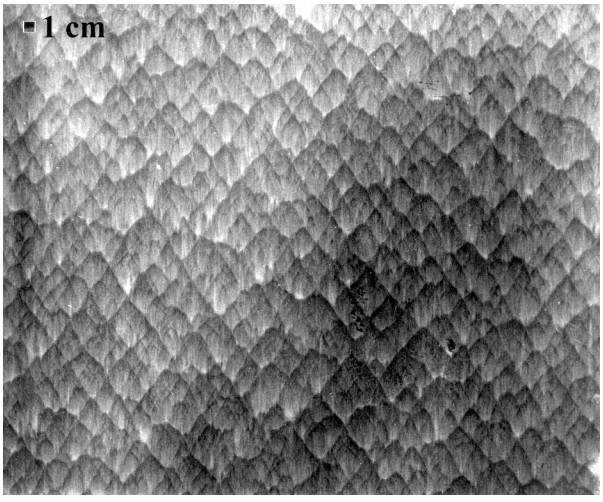

(c) β = 2, 40 kPa, Shot 910.

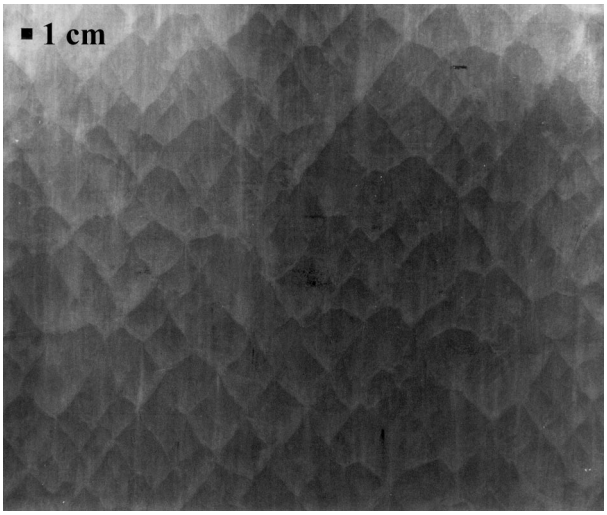

(d) β = 3.76, 100 kPa, Shot 926.

Fig. 17 Soot foils with cellular structure from propane-oxygen-nitrogen detonations.

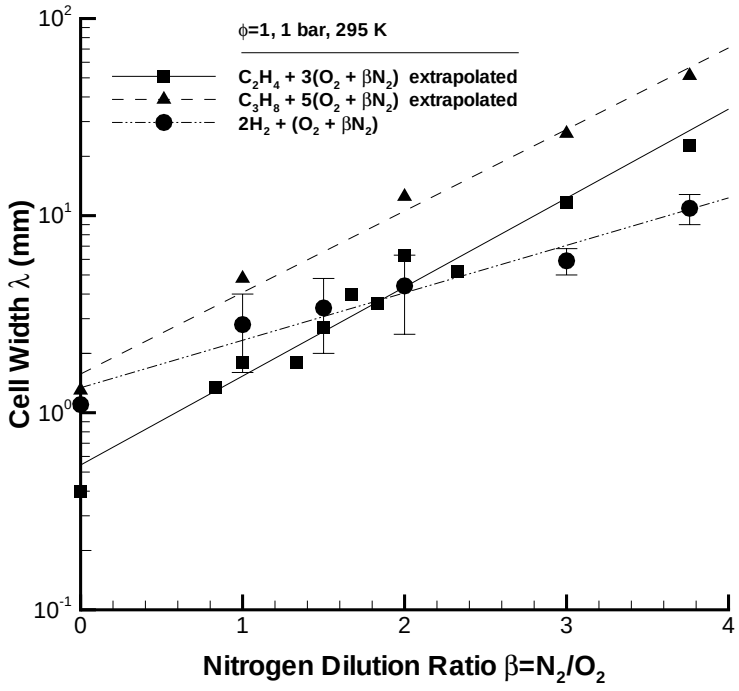

Fig. 18 Cell width data.

5 Conclusions

An preliminary experimental investigation into detonation diffraction with simulatneous propagation through a mixture gradient has been conducted. A brief summary of some of the previous research on these problems was presented. The initial series of diffraction experiments permitted documentation of the sub-critical, critical, and super-critical regimes via ruby laser shadowgraph and piezoelectric pressure transducers. In the second series of experiments, atmospheric pressure critical diffraction limits based on nitrogen dilution were identified for two types of experiments with hydrogen, ethylene, and propane fuels:

(1) Identical fuel-oxygen-nitrogen mixtures in the diffraction tube and test section.

(2) Fuel-oxygen in the diffraction tube and fuel-oxygen-nitrogen in the test section.

The sensitized (no nitrogen diluent) diffraction tube mixtures were able to initiate detonations in less sensitive (greater nitrogen concentration) test section mixtures compared to the experiments with identical mixtures in both. A final series of experiments was carried out to measure the detonation cell widths for the fuel-oxygen-nitrogen mixtures used throughout this study, due to the empirical correlations for critical tube diameter, critical initiation energy, and minimum tube diameter based on this length scale.

The problems of detonation diffraction and transmission through a mixture gradient require further analytical study independent of each other in order to achieve a fundamental understanding of the two. Experimentally, the two processes should be investigated under as wide a variety of conditions (i.e., mixture composition, initial thermodynamic state, degree of confinement or gradient, etc.) as possible to assist the development of analytical models. Details of how to characterize the cellular structure of a detonation and its effect on these problems should be carefully considered. Visualization tools such as high-speed framing camera photography and planar laser induced fluorescence (PLIF) will provide valuable information. The framing camera acquires many pictures during one experiment, permitting detailed study of the temporal and spatial evolution of a process. PLIF has the ability to delineate regions where chemical reactions are occurring, obviously important in the study of self-sustaining and perturbed detonations. Simultaneous shadowgraph and PLIF imaging would provide a nearly complete, instantaneous snapshot of the flowfield.

6 References

Bjerketvedt D, Sonju OK, Moen IO (1986) The influence of experimental condition on the reinitiation of detonation across an inert region. Dynamics of Explosions, Prog Astro Aero, 106:109-130.

Brinkley SR, Kirkwood JG (1947) Theory of the propagation of shock waves. Phys Rev, 71:606-611.

Bull DC, Elsworth JE, McLeod MA, Hughes D (1981) Initiation of unconfined gas detonations in hydrocarbon-air mixtures by a sympathetic mechanism. Prog Astro Aero, 75:61-72.

Desbordes D, Vachon M (1986) Critical diameter of diffraction for strong plane detonations. Dynamics of Explosions, Prog Astro Aero, 106:131-143.

Desbordes D, Guerraud C, Hamada L, Presles HN (1993) Failure of the classical dynamic parameters relationships in highly regular cellular detonation systems. Dynamics Aspects of Detonations, Prog Astro Aero, 153:347-359.

Edwards DH, Thomas GO, Nettleton MA (1979) The diffraction of a planar detonation wave at an abrupt area change. J Fluid Mech 95:79-96.

Edwards DH, Thomas GO (1981) Diffraction of a planar detonation in various fuel-oxygen mixtures at an area change. Prog Astro Aero 341-357.

Engebretsen T, Bjerketvedt D, Sonju OK (1993) Propagation of gaseous detonations through regions of low reactivity. Dynamics Aspects of Detonations, Prog Astro Aero, 153:324-346.

Guirao CH, Knystautas R, Lee J, Benedick W, Berman M (1982) Hydrogen-air detonations. 19th Symp (Intl) on Combustion, 583-590.

Knystautas R, Lee JH, Guirao CM (1982) The critical tube diameter for detonation failure in hydrocarbon-air mixtures. Comb Flame 48:63-83.

Lee JHS (1977) Initiation of gaseous detonation. Ann Rev Phys Chem 28:75-104

Lee JH, Matsui H (1977) A comparison of the critical energies for direct initiation of spherical detonations in acetylene-oxygen mixtures. Comb Flame 28:61-66.

Lee JH (1996) On the critical diameter problem. Dynamics of Exothermicity, ed Bowen JR. Gordon and Breech Publishers, Netherlands. 321-336.

Makris A, Oh TJ, Lee JHS, Knystautas R (1994) Critical diameter for the transmission of a detonation wave into a porous medium. 25th Symp (Intl) on Combustion, 65-71.

Matsui H (1979) On the measure of the relative detonation hazards of gaseous fuel-oxygen and air mixtures. 17th Symp (Intl) on Combustion, 1269-1280.

Moen IO, Donato M, Knystautas R, Lee JH (1981) The influence of confinement on the propagation of detonations near the detonability limits. 18th Symp (Intl) on Combustion, 1615-1622.

Moen IO, Murray SB, Bjerketvedt D, Rinnan A, Knystautas R, Lee JH (1982) Diffraction of detonation from tubes in a large fuel-air explosive cloud. 19th Symp (Intl) on Combustion, 635-644.

Moen IO, Funk JW, Ward SA, Rude GM, Thibault PA (1984) Detonation length scales for fuel-air explosives. Prog Astro Aero, 94:55-79.

Moen IO, Ward SA, Thibault PA, Lee JH, Knystautas R, Dean T, Westbrook CK (1985) The influence of diluents and inhibitors on detonations. 20th Symp (Intl) of Combustion, 1717-1726.

Moen IO, Sulmistras A, Thomas GO, Bjerketvedt D, Thibault PA (1986) Influence of cellular regularity on the behavior of gaseous detonations. Dynamics of Explosions, Prog Astro Aero 106:220-243.

Murray SB, Lee JH (1986) The influence of physical boundaries on gaseous detonation waves. Dynamics of Explosions, Prog Astro Aero 106:329-355.

Paterson S (1953) Contact transmission of detonation. 4th Symp (Int'l) on Combustion, 468-471.

Reynolds WC (1986) The element potential method for chemical equilibrium analysis: implementation in the interactive program STANJAN (3rd ed.). Mechanical Engineering Department, Stanford University.

Rinnan A (1982) Transmission of detonation through tubes and orifices. Fuel-Air Explosions, University of Waterloo Press, 553-564.

Shepherd JE, Moen IO, Murray SB, Thibault PA (1986) Analysis of the cellular structure of detonations. 21 Symp (Intl) on Combustion. 1649-1658.

Shepherd JE, Lee JHS (1992) On the transition from deflagration to detonation. Major Topics in Combustion, Springer-Verlag, 439-487.

Sloan SA, Nettleton MA (1975) A model for the axial decay of a shock wave in a large abrupt area change. J Fluid Mech, 71:769-784.

Soloukhin RI, Ragland KW (1969) Ignition processes in expanding detonations. Comb Flame 13:295-302.

Strehlow RA (1970) Multi-dimensional detonation wave structure. Astronautica Acta, 15:345-357.

Strehlow RA, Adamczyk AA, Stiles RJ (1972) Transient studies of detonation waves. Astronautica Acta, 17:509-527.

Strehlow RA (1984) Combustion fundamentals. McGraw-Hill. 302-337, 396-410.

Thomas GO, Edwards DH, Lee JH, Knystautas R, Moen IO, Wei YM (1986) Detonation diffraction by divergent channels. Dynamics of Explosions, Prog Astro Aero, 106:144-154.

Thomas GO, Sutton P, Edwards DH (1991) The behavior of detonation waves at concentration gradients. Combustion and Flame, 84:312-322.

Thompson, PA (1988) Compressible-Fluid Dynamics. 495-502.

Urtiew PA, Tarver CM (1981) Effects of cellular structure on the behavior of gaseous detonation waaves under transient conditions. Prog Astro Aero 371-384.

Whitham GB (1957) A new approach to problems of shock dynamics: Part I, two-dimensional problems. J Fluid Mech, 2:145-171.

Zeldovich IaB, Kogarko SM, Simonov NN (1956) An experimental investigation of spherical detonation in gases. Sov Phys Tech Phys, 1:1689-1713.

Appendix A: One Mixture Diffraction Data

Table 4: Hydrogen-oxygen-nitrogen one mixture diffraction experiment data.

Shot #	P_1 (kPa)	β	ϕ	V_{CJ} (m/s)	P_{CJ} (bar)	T_{CJ} (K)	V_{avg} (m/s)	$\%V_{CJ}$ deficit	Criticality	Visualization
719	100	0.50	1	2568	18.3	3558	2532	-1.40	super	ruby
720	100	1.00	1	2400	18.3	3453	2381	-0.79	sub	ruby
721	100	0.75	1	2476	18.5	3505	2454	-0.89	sub	ruby
722	100	0.63	1	2520	18.7	3532	2500	-0.79	super	ruby

Table 5: Ethylene-oxygen-nitrogen one mixture diffraction experiment data.

Shot #	P_1 (kPa)	β	ϕ	V_{CJ} (m/s)	P_{CJ} (bar)	T_{CJ} (K)	V_{avg} (m/s)	$\%V_{CJ}$ deficit	Criticality	Visualization
856	100	0.67	1	2178	28.4	3667	2180	0.09	super	ruby
857	100	1.00	1	2114	26.5	3561	2116	0.09	super	ruby
858	100	1.33	1	2061	25	3465	2062	0.05	sub	ruby
859	100	1.17	1	2086	25.7	3511	2089	0.12	sub	ruby
860	100	1.07	1	2102	26.2	3541	2105	0.14	sub	ruby

Table 6: Propane-oxygen-nitrogen one mixture diffraction experiment data.

Shot #	P_1 (kPa)	β	ϕ	V_{CJ} (m/s)	P_{CJ} (bar)	T_{CJ} (K)	V_{avg} (m/s)	%V_{CJ} deficit	Criticality	Visualization
818	100	0.50	1	2199	31.1	3620	2198	-0.05	super	none
819	100	0.70	1	2154	29.4	3551	2145	-0.42	sub	ruby
820	100	0.60	1	2176	30.2	3585	2174	-0.09	sub	ruby
821	100	0.50	1	2199	31.1	3620	2198	-0.07	super	ruby
822	100	0.56	1	2185	30.5	3599	2192	0.32	super	ruby

Appendix B: Two Mixture Diffraction Data

Table 7: Hydrogen-oxygen-nitrogen two mixture diffraction experiment data.

		Diffraction Tube							Test Section						
Shot #	P_1 (kPa)	β	ϕ	V_{CJ} (m/s)	P_{CJ} (bar)	T_{CJ} (K)	V_{avg} (m/s)	$\%V_{CJ}$ deficit	β	ϕ	V_{CJ} (m/s)	P_{CJ} (bar)	T_{CJ} (K)	Criticality	Visualization
738	100	0.00	1	2842	18.9	3683	2847	0.18	0.00	1	2842	18.9	3683	super	ruby
741	100	0.00	1	2842	18.9	3683	2837	-0.18	0.00	1	2842	18.9	3683	super	ruby
743	100	0.00	1	2842	18.9	3683	2827	-0.53	0.00	1	2842	18.9	3683	super	ruby
746	100	0.00	1	2842	18.9	3683	2817	-0.88	1.25	1	2335	18.1	3402	sub	none
747	100	0.00	1	2842	18.9	3683	2817	-0.88	1.25	1	2335	18.1	3402	super	ruby
748	100	0.00	1	2842	18.9	3683	2817	-0.88	1.40	1	2301	18.2	3374	sub	ruby
749	100	0.00	1	2842	18.9	3683	2817	-0.88	1.30	1	2324	18.3	3394	sub	ruby

Table 8: Ethylene-oxygen-nitrogen two mixture diffraction experiment data.

		Diffraction Tube							Test Section						
Shot #	P_1 (kPa)	β	ϕ	V_{CJ} (m/s)	P_{CJ} (bar)	T_{CJ} (K)	V_{avg} (m/s)	$\%V_{CJ}$ deficit	β	ϕ	V_{CJ} (m/s)	P_{CJ} (bar)	T_{CJ} (K)	Criticality	Visualization
763	100	0.00	1	2377	34.8	3943	2374	-0.13	0.67	1	2178	28.4	3667	super	ruby
764	100	0.00	1	2377	34.8	3943	2374	-0.13	0.87	1	2138	27.2	3602	super	none
765	100	0.00	1	2377	34.8	3943	2381	0.17	1.07	1	2145	27.2	3521	super	ruby

Table 8: Ethylene-oxygen-nitrogen two mixture diffraction experiment data.

		Diffraction Tube							Test Section						
Shot #	P_1 (kPa)	β	ϕ	V_{CJ} (m/s)	P_{CJ} (bar)	T_{CJ} (K)	V_{avg} (m/s)	$\%V_{CJ}$ deficit	β	ϕ	V_{CJ} (m/s)	P_{CJ} (bar)	T_{CJ} (K)	Criticality	Visualization
766	100	0.00	1	2377	34.8	3943	2374	-0.13	1.33	1	2061	25	3465	sub	ruby
767	100	0.00	1	2377	34.8	3943	2374	-0.13	1.27	1	2071	25.3	3483	super	ruby

Table 9: Propane-oxygen-nitrogen two mixture diffraction experiment data.

		Diffraction Tube							Test Section						
Shot #	P_1 (kPa)	β	ϕ	V_{CJ} (m/s)	P_{CJ} (bar)	T_{CJ} (K)	V_{avg} (m/s)	$\%V_{CJ}$ deficit	β	ϕ	V_{CJ} (m/s)	P_{CJ} (bar)	T_{CJ} (K)	Criticality	Visualization
753	100	0.00	1	2362	37.7	3834	2360	-0.08	0.00	1	2362	37.7	3834	super	ruby
755	100	0.00	1	2362	37.7	3834	2353	-0.38	0.40	1	2225	32.1	3657	super	ruby
759	100	0.00	1	2362	37.7	3834	2353	-0.38	0.56	1	2251	32.4	3604	super	ruby
760	100	0.00	1	2362	37.7	3834	2360	-0.08	0.80	1	2133	28.7	3519	sub	ruby
761	100	0.00	1	2362	37.7	3834	2353	-0.38	0.72	1	2204	30.8	3541	super	ruby
762	100	0.00	1	2362	37.7	3834	2346	-0.68	0.76	1	2190	29.7	3296	sub	ruby

Appendix C: Diffraction Shadowgraphs

Hydrogen-oxygen-nitrogen one mixture diffraction shadowgraphs

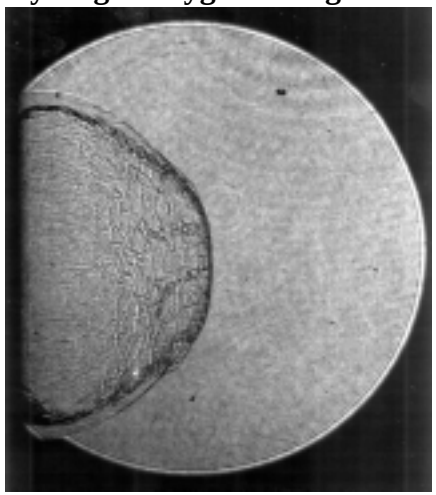

Shot 719, $\beta = 0.5$

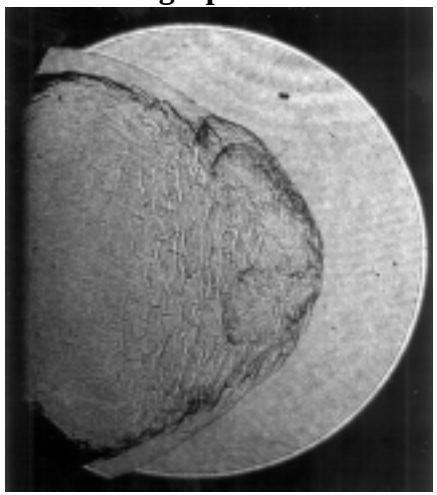

Shot 722, $\beta = 0.63$

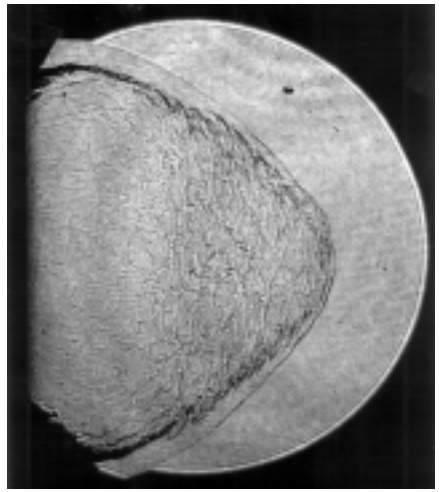

Shot 721, $\beta = 0.75$

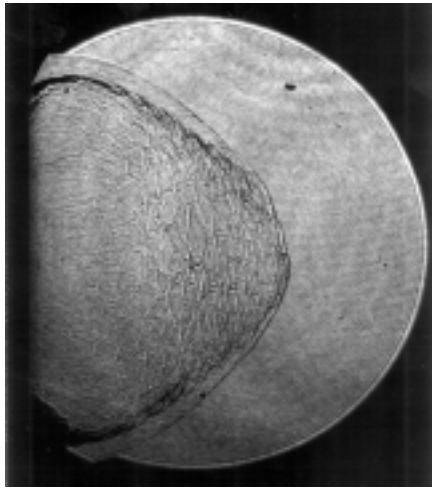

Shot 720, $\beta = 1.0$

Ethylene-oxygen-nitrogen one mixture diffraction shadowgraphs

Shot 856, $\beta = 0.67$

Shot 857, $\beta = 1.0$

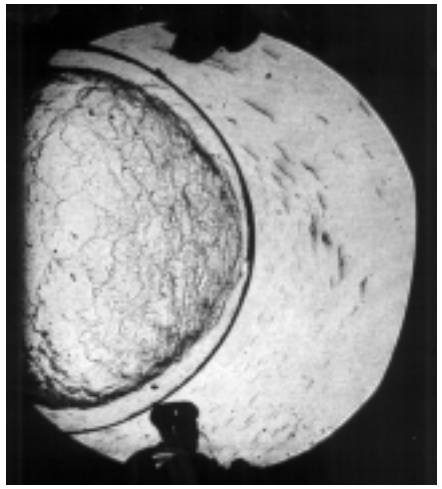

Shot 860, $\beta = 1.07$

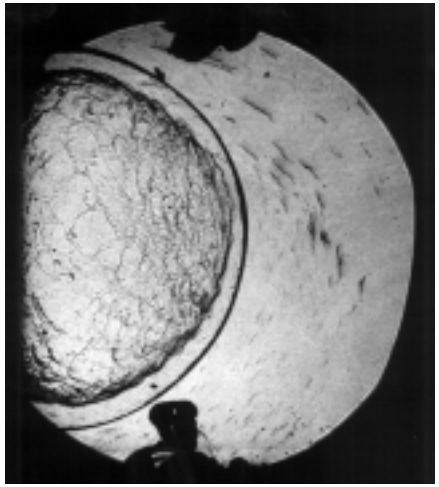

Shot 859, $\beta = 1.17$

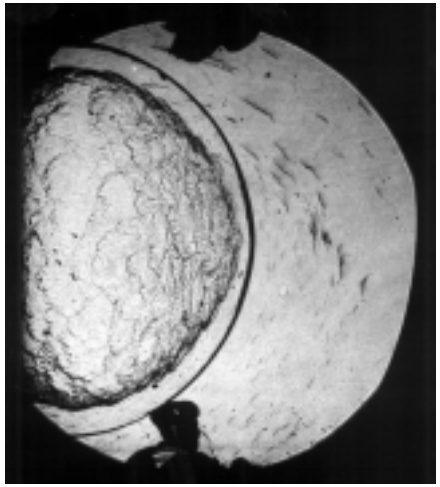

Shot 858, $\beta = 1.33$

Propane-oxygen-nitrogen one mixture diffraction shadowgraphs

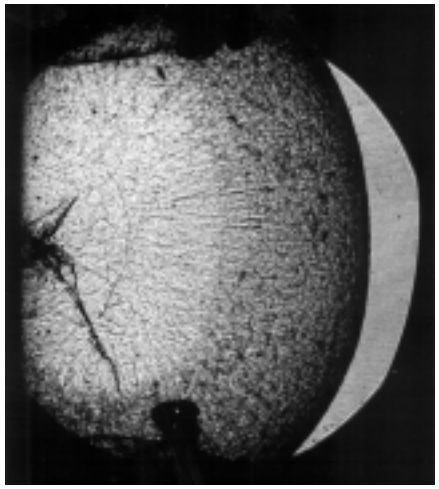

Shot 821, $\beta = 0.5$

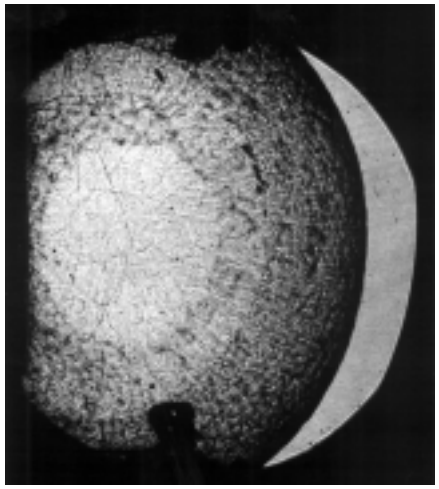

Shot 822, $\beta = 0.56$

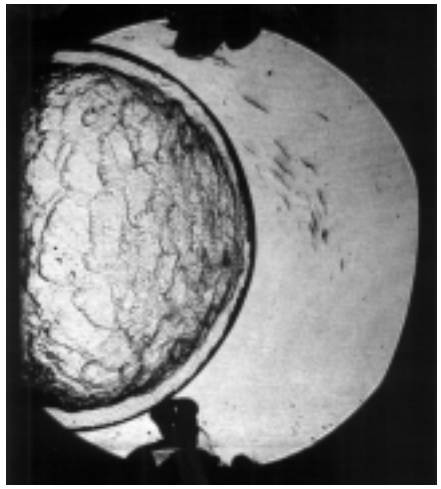

Shot 820, $\beta = 0.6$

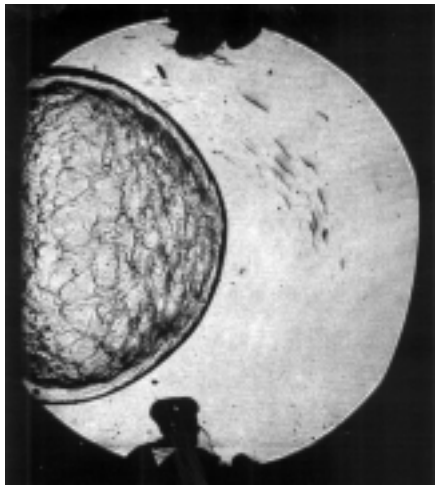

Shot 819, $\beta = 0.7$

Hydrogen-oxygen-nitrogen two mixture diffraction shadowgraphs

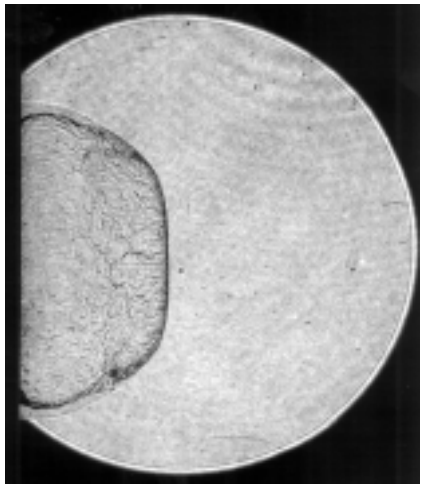

Shot 738, β = 0.0

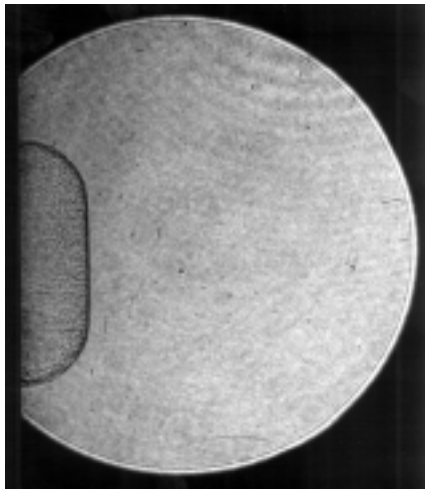

Shot 741, β = 0.0

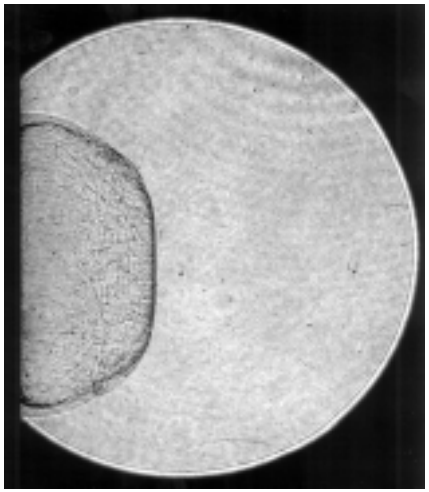

Shot 743, β = 0.0

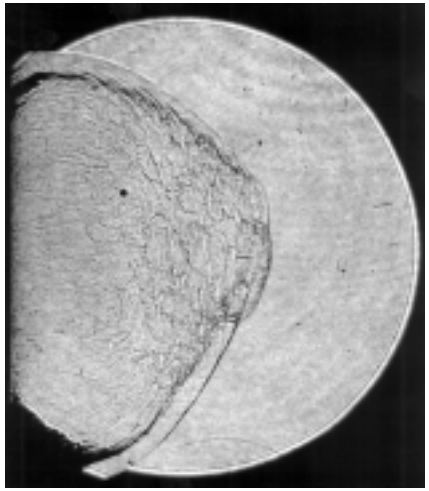

Shot 747, β = 1.25

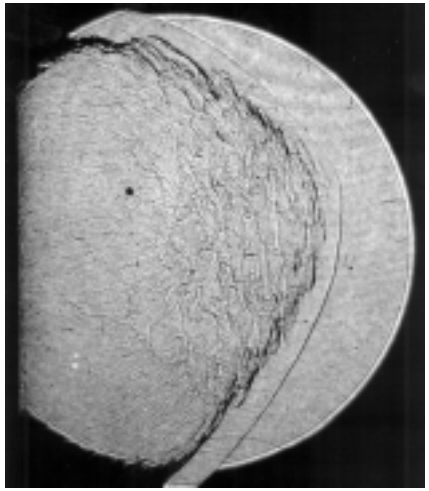

Shot 749, β = 1.3

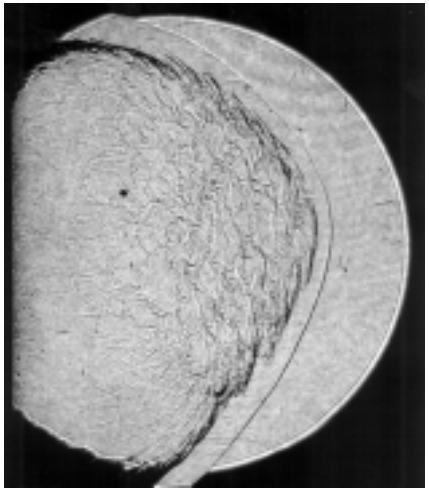

Shot 748, β = 1.4

Ethylene-oxygen-nitrogen two mixture diffraction shadowgraphs

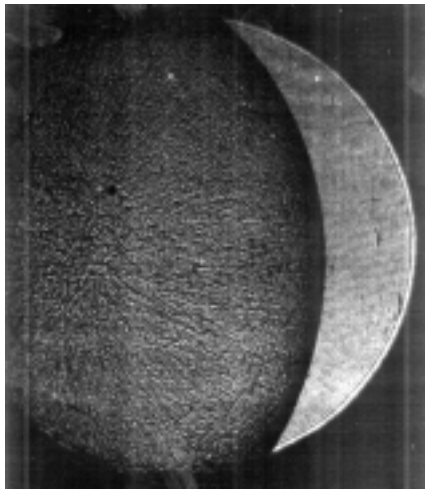

Shot 763, $\beta = 0.67$

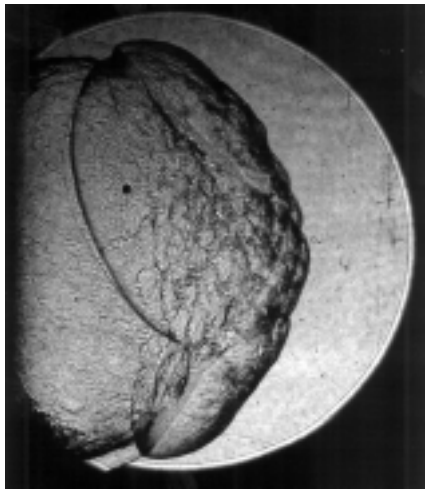

Shot 765, $\beta = 1.07$

Shot 767, $\beta = 1.27$

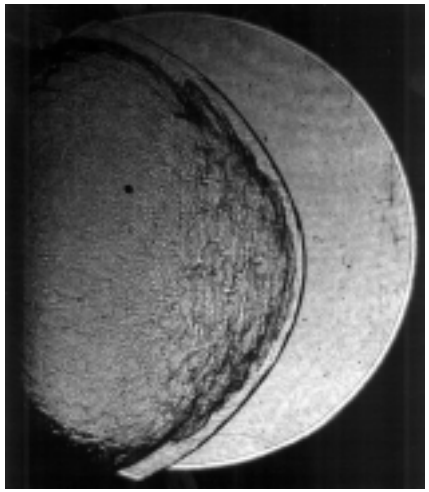

Shot 766, $\beta = 1.33$

Propane-oxygen-nitrogen two mixture diffraction shadowgraphs

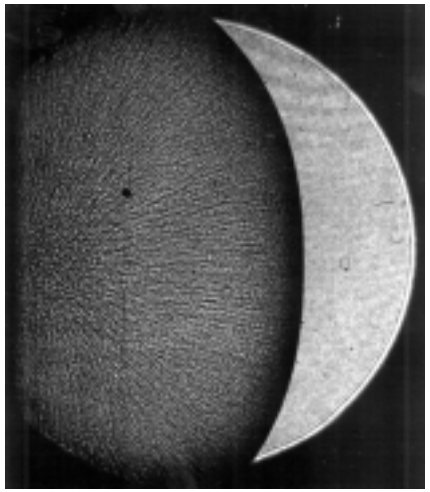

Shot 753, $\beta = 0.0$

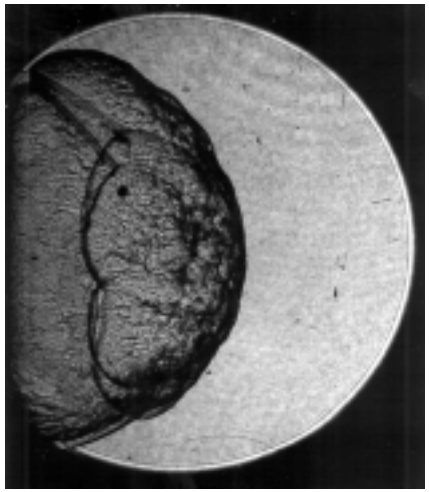

Shot 755, $\beta = 0.4$

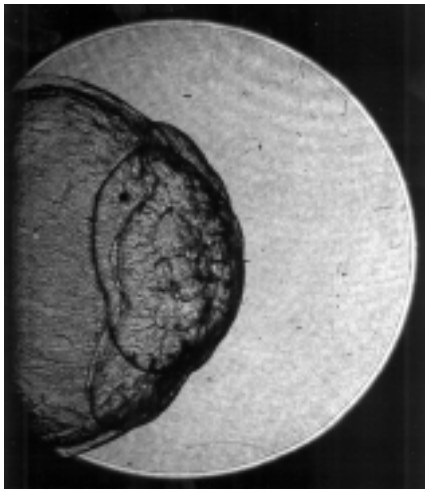

Shot 759, $\beta = 0.56$

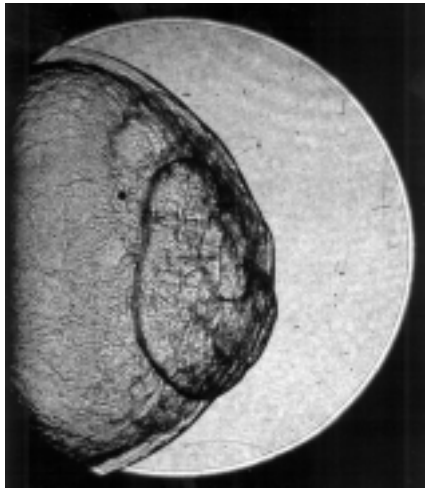

Shot 761, $\beta = 0.72$

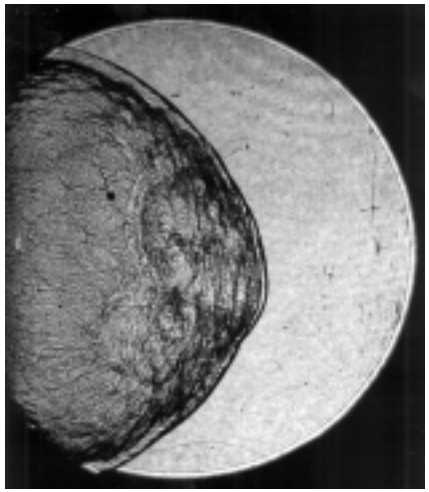

Shot 762, $\beta = 0.76$

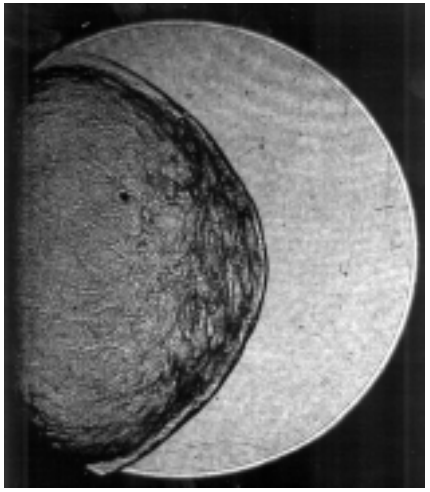

Shot 760, $\beta = 0.8$

Appendix D: Cellular Structure Data

Table 10: Hydrogen cellular structure experimental data.

Shot #	P_1 (kPa)	β	ϕ	V_{CJ} (m/s)	P_{CJ} (bar)	T_{CJ} (K)	V_{avg} (m/s)	%V_{CJ} deficit	λ_{min} (mm)	λ_{max} (mm)	λ_{avg} (mm)
522	101.5	1.00	1	2398	18.1	3452	2416	0.8	2.5	4	3
523	51.5	1.00	1	2370	8.9	3350	2387	0.7	4	6	4.9
530	41	1.00	1	2360	7.1	3317	2376	0.7	4.5	6.5	5.5
531	26.5	1.00	1	2341	4.4	3250	2353	0.5	6	11	8.7
532	11.5	1.00	1	2303	1.7	3122	2310	0.3	16	36.5	25.3
533	50.9	2.00	1	2164	8.5	3176	2176	0.6	4	7.5	5.9
534	57.2	2.00	1	2168	9.5	3190	2181	0.6	5	8	6.2
535	84.6	3.00	1	2046	13.6	3062	2058	0.6	5.5	8	6.5
536	51.5	3.00	1	2033	8.1	3016	2040	0.4	7.5	12	9.5
537	101.5	3.00	1	2051	16.4	3079	2060	0.5	5	6.5	5.9
538	101.5	2.00	1	2187	17.3	3258	2201	0.6	2.5	6	4.4
539	26.5	2.00	1	2141	4.2	3095	2151	0.5	9	14.5	11.7
540	26.5	3.00	1	2014	4	2951	2017	0.1	11	17	14.3
541	26.5	3.00	1	2014	4	2951	2018	0.2	11	17	13.7
542	10	1.00	1	2302	1.7	3119	2300	-0.1	25.5	36.5	29.1
543	100	1.00	1	2398	18.1	3452	2415	0.7	2	4	2.8
544	83.1	3.00	1	2046	13.4	3061	2055	0.4	5	7.5	6.2
551	39.5	1.00	1	2395	6.9	3314	2373	-0.9	4.5	7.5	5.9

Table 10: Hydrogen cellular structure experimental data.

Shot #	P_1 (kPa)	β	ϕ	V_{CJ} (m/s)	P_{CJ} (bar)	T_{CJ} (K)	V_{avg} (m/s)	%V_{CJ} deficit	λ_{min} (mm)	λ_{max} (mm)	λ_{avg} (mm)
556	25	1.00	1	2341	4.4	3250	2348	0.3	6	10.5	8.25
557	50	1.00	1	2370	9	3350	2385	0.7	3.5	5	4.25
558	49.4	2.00	1	2164	8.4	3175	2175	0.5	5.5	7	6.5
559	55.7	2.00	1	2167	9.5	3188	2179	0.5	4.5	6	5.3
880	100	3.76	1	1972	16.2	2949	1981	0.5	9	12	10.9
881	50	0.00	1	2804	9.42	3555	2814	0.3	3	5	4
882	85	0.50	1	2561	15.6	3530	2577	0.6	1	3	2.1
883	65	0.25	1	2664	12.2	3542	2678	0.5	1	3	2.1
884	100	0.00	1	2843	19.6	3687	2853	0.3	0.5	2	1.1
885	100	1.50	1	2280	18.1	3355	2291	0.5	2	4	3.4

Table 11: Ethylene cellular structure experimental data.

Shot #	P_1 (kPa)	β	ϕ	V_{CJ} (m/s)	P_{CJ} (bar)	T_{CJ} (K)	V_{avg} (m/s)	%V_{CJ} deficit	λ_{min} (mm)	λ_{max} (mm)	λ_{avg} (mm)
693	31.5	1.67	1	1978	7	3227	1990	0.6	5.5	10	7.2
694	80	1.67	1	2009	18.7	3346	2022	0.7	4	6	5
695	50	1.67	1	1994	11.5	3287	2007	0.6	4.5	6.5	5.4
696	40	1.67	1	1987	9.2	3259	1998	0.6	4.5	7	5.7
697	45	1.67	1	1990	10.3	3274	2002	0.6	4	6.5	5.6

Table 11: Ethylene cellular structure experimental data.

Shot #	P_1 (kPa)	β	ϕ	V_{CJ} (m/s)	P_{CJ} (bar)	T_{CJ} (K)	V_{avg} (m/s)	%V_{CJ} deficit	λ_{min} (mm)	λ_{max} (mm)	λ_{avg} (mm)
698	35	1.67	1	1983	8	3243	1995	0.6	5.5	7.5	6.3
710	46.5	1.83	1	1971	10.4	3239	1985	0.7	5.5	9.5	7.8
711	45	1.50	1	2011	10.6	3313	2023	0.6	4.5	7	5.9
712	45	2.00	1	1954	9.9	3201	1964	0.5	6	11	8
713	45	1.33	1	2052	10.8	3353	2046	-0.3	3.5	5	4
890	50	0.00	1	2343	16.7	3794	2356	0.6	0.5	1	0.8
891	15	0.00	1	2286	4.8	3559	2283	-0.1	1	3	2.1
892	30	1.00	1	2070	7.5	3377	2075	0.2	3	7	4.9
893	70	1.00	1	2100	18.1	3504	2115	0.7	2	4	2.6
894	60	2.00	1	1963	13.3	3233	1972	0.5	8	12	9.3
895	80	2.00	1	1971	17.9	3267	1978	0.3	6	11	7.9
896	50	3.00	1	1867	9.9	3012	1872	0.3	19	23	20.1
897	90	3.00	1	1881	18.1	3064	1890	0.5	9	17	12.9
898	50	3.76	1	1811	9.3	2876	1784	-1.5	29	43	37.4
899	100	3.76	1	1825	19.1	2927	1832	0.4	19	29	22.8
928	55	1.67	1	1997	12.7	3299	2009	0.6	6	9	7
929	30	1.67	1	1978	6.8	3223	1987	0.5	7.5	11	9
930	50	0.83	1	2116	13.2	3500	2130	0.6	2	3.5	2.7
931	50	2.33	1	1924	10.6	3143	1933	0.5	8.5	12.5	10.4

Table 12: Propane cellular structure experimental data.

Shot #	P_1 (kPa)	β	ϕ	V_{CJ} (m/s)	P_{CJ} (bar)	T_{CJ} (K)	V_{avg} (m/s)	%V_{CJ} deficit	λ_{min} (mm)	λ_{max} (mm)	λ_{avg} (mm)
548	50	0.00	1	2329	18.1	3697	2329	0.0	2	3	2.5
549	25	0.00	1	2298	8.8	3569	2307	0.4	3	4.5	3.7
550	15	0.00	1	2275	5.2	3478	2287	0.5	4	7	5.5
908	35	0.00	1	2312	12	3623	2322	0.4	2	4	2.8
909	30	1.00	1	2055	7.8	3290	2063	0.4	9	21	13.3
910	40	2.00	1	1933	8.9	3097			22	38	29.2
911	80	2.00	1	1952	18.2	3169	1964	0.6	12	19	15.6
912	70	1.00	1	2084	18.7	3406	2098	0.7	4	10	6.8
913	50	3.00	1	1847	10	2919	1848	0.1	40	50	46.8
914	90	3.00	1	1857	16.1	2956	1869	0.7	23	36	29
915	50	3.76	1	1789	9.3	2780	1789	0.0	66	90	78
926	100	3.76	1	1801	18.9	2824	1799	-0.1	41	63	51.3